npj | biofilms and microbiomes

Article

Published in partnership with Nanyang Technological University

https://doi.org/10.1038/s41522-025-00693-y

EPS inhibitor treatment of *Salmonella* impacts evolution without selecting for resistance to biofilm inhibition

Mathieu Joos[1,5], Sybren Van Ginneken[1,5], Xabier Villanueva[1], Marie Dijkmans[1], Guglielmo A. Coppola[1,2], Camilo Andres Pérez-Romero[3], Thijs Vackier[1], Erik Van der Eycken[2,4], Kathleen Marchal[3], Bram Lories[1,6] & Hans P. Steenackers[1,6] ✉

Virulence factors of pathogens, such as toxin production and biofilm formation, often exhibit a public character, providing benefits to nearby non-producers. Consequently, anti-virulence drugs targeting these public traits may not select for resistance, as resistant mutants that resume production of the virulence factor share the benefits of their resistance with surrounding sensitive cells. In agreement with this, we show that even after long-term treatment with a 2-amino-imidazole (2-AI) biofilm inhibitor, *Salmonella* populations remained as susceptible to biofilm inhibition as the ancestral populations. Nonetheless, further genotypic and phenotypic analysis revealed that the *Salmonella* populations did adapt to the treatment and accumulated mutations in efflux pump regulators and alternative sigma factors. These mutations resulted in a reduced biofilm-forming capacity and increased efflux activity. Their selection was due to a growth delaying side effect of the biofilm inhibitor. Enhanced efflux activity helped overcome this growth delay, providing a fitness advantage over the ancestor. Finally, we demonstrate that chemical modification of the inhibitor enhances its specificity by partially alleviating the unintended growth delay while retaining the anti-biofilm activity, which in turn eliminated the selection pressure for increased efflux. Overall, our findings highlight that while unintended side effects can complicate anti-virulence strategies, adaptation to these effects does not necessarily restore the inhibited virulence trait. Moreover, chemical modification can mitigate these unintended side effects and enhance drug specificity.

Conventional antibiotics either directly compromise bacterial cell viability (e.g., β-lactams) or target processes essential for cell division, such as DNA replication (e.g., fluoroquinolones)[1]. Because of the essential nature of these antibiotic targets, mutations conferring resistance are rapidly selected for upon antibiotic exposure[2–4]. Therefore, the development of anti-virulence drugs has gained interest. Unlike conventional antibiotics, anti-virulence drugs do not directly target bacterial viability or replication. Instead, they inhibit virulence factors that pathogens rely on to establish infections and cause disease within a host[5]. Since virulence factors are non-essential, the potential fitness benefit of resistant mutants that resume expression of the virulent trait during drug treatment is predicted to be more limited compared to conventional antibiotics. Consequently, inhibiting virulence factors should impose a reduced selective pressure for resistance compared to classical antibiotics[6]. Moreover, virulence factors frequently act as public goods, providing benefits that are shared within a population[7]. According to social evolution theory, targeting a public good virulence factor with an inhibitor creates selective pressure against the emergence of resistance[8,9]. In such cases, resistant mutants that restore the production of the public good bear the metabolic cost of its production, while the benefits are exploited by sensitive "cheater" cells that do not contribute to its synthesis. This dynamic results in a net negative fitness effect for resistant mutants, leading to their counter-selection within the population.

Biofilms, which are microbial communities embedded within a self-produced matrix of exopolymeric substances (EPS)[10,11], represent a

[1]KU Leuven - MiCA Lab, Centre of Microbial and Plant Genetics, Leuven, Belgium. [2]Department of Chemistry, KU Leuven - Laboratory for Organic & Microwave-Assisted Chemistry (LOMAC), Leuven, Belgium. [3]Department of Plant Biotechnology and Bioinformatics, UGent – Internet Technology and Data Science Lab (IDLab), Gent, Belgium. [4]People's Friendship University of Russia (RUDN University), Moscow, Russia. [5]These authors contributed equally: Mathieu Joos, Sybren Van Ginneken.[6]These authors jointly supervised this work: Bram Lories, Hans P. Steenackers. ✉e-mail: hans.steenackers@kuleuven.be

compelling target for anti-virulence strategies. Bacterial cells encased within a biofilm matrix are protected against both the host immune system and antimicrobial therapies, making biofilm-associated infections persistent and difficult to eradicate[12]. Beyond enhancing tolerance, biofilm matrix components can further contribute to virulence by, for example, promoting adhesion and cell invasion or by exacerbating inflammation[13–15]. Moreover, previous research has demonstrated that biofilm components can enable nearby non-producers to integrate into the biofilm and benefit from its protective properties, establishing that biofilm components can act as public goods[7,16,17].

In this context, we have developed a group of 5-aryl-2-aminoimidazole-based (2-AI) EPS inhibitors[7,18–23]. These 2-AI's repress EPS production and biofilm formation in a broad spectrum of micro-organisms, including the enteric pathogen *Salmonella* Typhimurium[20,23]. In *Salmonella*, 2-AI's inhibit biofilm formation by repressing the transcriptional activator CsgD, preventing the biosynthesis of curli fimbriae and cellulose[22]. These EPS components are required for *Salmonella* biofilm formation and can contribute to other virulence traits such as adhesion, cell invasion, and inflammation[13,15,24]. Consistent with the theory outlined above, we showed that *Salmonella* did not develop resistance —defined as the ability to resume EPS production and biofilm formation during inhibitor treatment— after repeated exposure to the inhibitor[7]. While we did not observe resistance to EPS inhibition, we did not further explore if long-term 2-AI treatment affected other traits of the exposed biofilms. Therefore, the goal of the current study was to investigate in more detail how *Salmonella* biofilms adapt to long-term treatment with an EPS inhibitor on a genotypic and phenotypic level.

Results

Long-term treatment with an EPS inhibitor does not select for resistance to biofilm inhibition in *Salmonella* Typhimurium

Previous work has demonstrated that 5-(4-chlorophenyl)-N-cyclopentyl-1H-imidazol-2-amine (RC41; Supplementary Fig. 1A) acts as a potent 2-aminoimidazole-based (2-AI) EPS inhibitor. It strongly represses the expression of *csgD*[22], the master regulator for biofilm formation in *Salmonella*, thereby reducing biofilm formation[7]. As unintended side effects of this EPS inhibitor on planktonic growth could influence resistance development, a dose-response curve quantifying the effect on both biofilm biomass and planktonic biomass was first determined (Fig. 1A). For concentrations lower than 20 μM, no effect was observed: both planktonic biomass and biofilm biomass were comparable to those of untreated cultures after 48 h. For concentrations between 20 μM and 80 μM, a dose-dependent inhibition of biofilm biomass was observed. This reduction in biofilm biomass corresponded to an increase in planktonic biomass, indicating a shift from cells in the biofilm phase on the pegs to the planktonic phase in the wells. For higher concentrations (≥100 μM), an almost complete (≥99%) inhibition of biofilm biomass was observed. However, at these concentrations, planktonic biomass was also reduced, indicating that there is an unintended side effect of the EPS inhibitor on planktonic growth at these elevated concentrations. Based on these results, a concentration of 50 μM was selected for long-term treatment, as this concentration substantially reduced biofilm biomass (±75% inhibition), while no reduction of planktonic biomass was observed (Fig. 1B, C).

Next, a serial passage evolution experiment, similar to the experiment conducted by Dieltjens et al.[7], was performed to evaluate how *Salmonella* populations adapt to long-term treatment with an EPS inhibitor. *Salmonella* biofilms were grown on the bottom of Petri dishes filled with diluted TSB broth, mimicking the development of biofilms on nutrient-limiting industrial surfaces such as conveyer belts in the food industry. After 48 h, the biofilms were scraped off and used to inoculate a new cycle. This process was repeated for 20 cycles, corresponding to an experimental duration of 40 days. In addition to three independent RC41-treated lineages (50 μM), three control lineages (0 μM) were included to distinguish between adaptations specific to inhibitor treatment and adaptations to the general biofilm setup. After repeated treatment, resistance development against the EPS inhibitor was evaluated (Fig. 1D–F), with resistance defined as the ability to form biofilms during treatment. Inhibitor treatment still reduced biofilm biomass of the RC41-evolved populations by ±73% (Fig. 1D), which is comparable to the inhibition observed for wild-type *Salmonella* (±77%). Moreover, absolute biofilm biomass levels (Fig. 1F) after inhibitor treatment of the three RC41-evolved populations (0.047 OD_{570nm}) remained as low as the biofilm biomass levels of treated wild-type (0.073 OD_{570nm}) and control-evolved populations (0.026 OD_{570nm}). We obtained similar results when these experiments were performed using individual clones isolated from the evolved populations rather than population-level samples (Supplementary Fig. 2). In addition, no differences in planktonic biomass were observed between the different groups after RC41 treatment (Fig. 1E). Taken together, these observations confirm our previous results and show that 40 days of treatment with an EPS inhibitor does not result in resistance against the anti-biofilm effect in *Salmonella* biofilms[7].

Long-term treatment with an EPS inhibitor selects for mutations in efflux pump regulators and components of the RNA polymerase complex

Although no resistance against the anti-biofilm activity of the EPS inhibitor was observed, we hypothesized that long-term EPS inhibition could still impact evolutionary dynamics in bacterial populations. To investigate how the *Salmonella* biofilms adapted to long-term treatment with the EPS inhibitor, the genomic DNA of the evolved biofilms was extracted and subjected to whole-genome sequencing. In Table 1, an overview is given of the mutations present in the RC41-evolved populations. Only mutations that appeared with a frequency equal to or above 10% and that did not appear (<1%) in the parental cultures or control-evolved populations are shown. Mutations that were also present in the control-evolved populations are likely not specific adaptations to inhibitor treatment but rather adaptations to the general biofilm setup instead. A full list of all identified mutations can be found in Supplementary Data. Overall, we identified on average 10 mutations above the imposed 10% threshold in the RC41-evolved populations (RC41-1 = 8; RC41-2 = 11; RC41-3 = 11). In contrast, only 5 mutations were found on average in the control populations (C1 = 5; C2 = 6; C3 = 3).

All three RC41-evolved populations contained a high frequency of mutations related to the *ramR* gene. RamR is an AcrR-like transcriptional regulator, which, upon dimerization, binds upstream of and represses the expression of *ramA*[25]. RamA is a transcriptional activator of the AcrAB-TolC efflux pump, making RamR an indirect repressor of this efflux system (Fig. 2A)[26,27]. The AcrAB system is the major RND-type, broad-substrate efflux pump in *S.* Typhimurium, and its overexpression is responsible for low resistance levels to various antimicrobials[28]. The identified mutations either map to the RamR binding site upstream of *ramA*, the dimerization interface of RamR (Trp185*), or the DNA binding region of RamR (Thr50Pro, Leu58Trp) (Fig. 2B). RamR mutations similar to the ones described here are commonly reported in multi-drug resistant isolates of *Salmonella* and related *Enterobacteriaceae*[26,29–31]. They generally cause a reduction in RamR-mediated repression of *ramA*, resulting in accumulation of RamA and consequently an overexpression of the AcrAB efflux pump[29–31]. We, therefore, expect that the observed *ramR* mutations have a similar effect, causing increased efflux levels through reduced repression of *acrAB*.

In addition, mutations in the RNA polymerase (RNAP) complex were also found in all three independently evolved *Salmonella* biofilms treated with the EPS inhibitor, albeit at lower frequencies compared to the *ramR* mutations (Fig. 2C). In lineages 2 and 3, mutations were found in the *rpoS* gene, which encodes the stationary phase sigma factor σ^S (Fig. 2D). The observed mutations include a frameshift early on in the protein sequence (Asp37fs) and a specific point mutation (Trp149Arg) in the DNA binding interface. The Trp149 residue plays a key role in the interaction of σ^S with the -10 promoter element, and substitution of this residue with a different amino acid (including the exact Arg substitution observed here) has been demonstrated to abolish σ^S functionality[32]. Thus, both these *rpoS* mutations

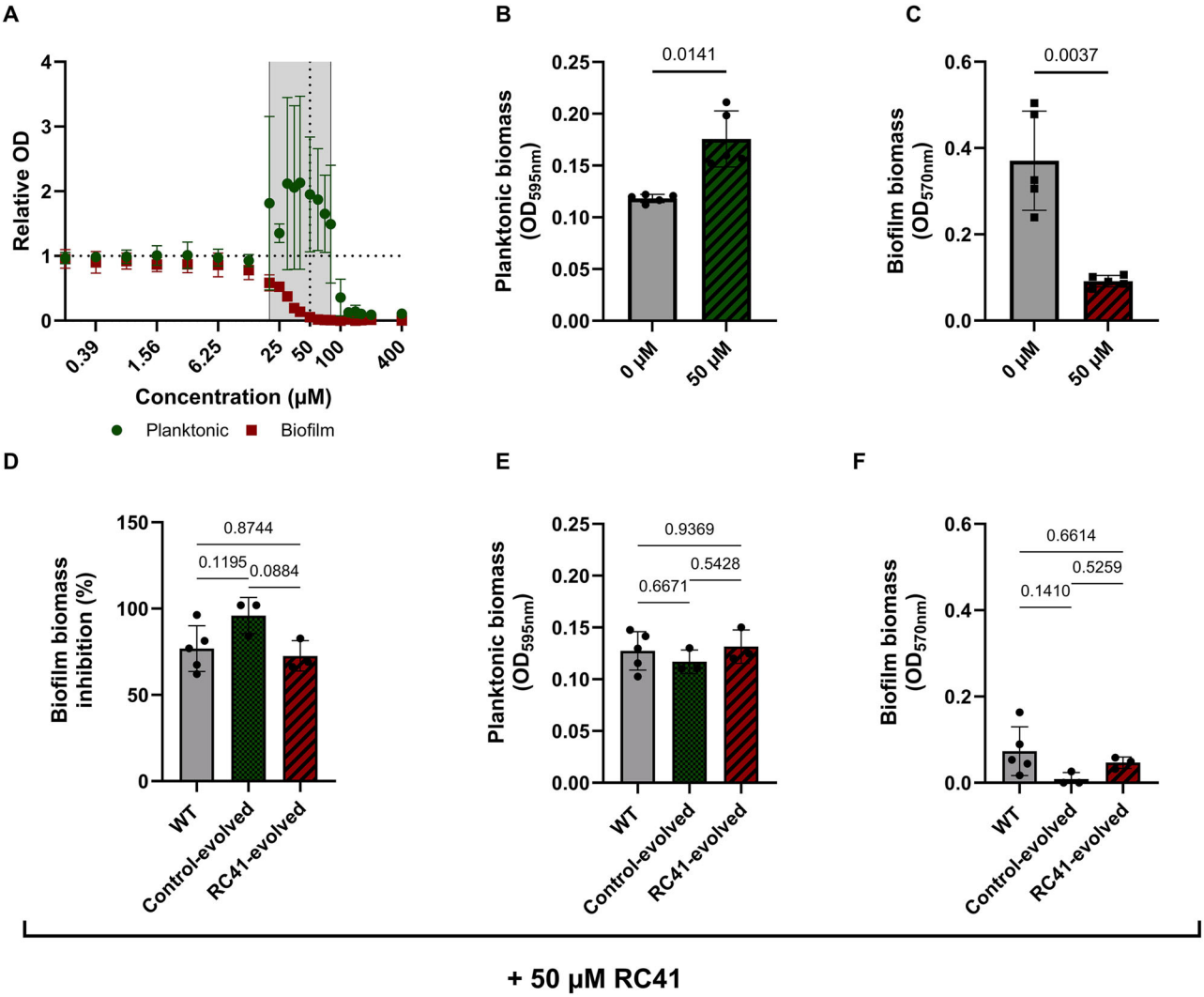

Fig. 1 | Long-term EPS inhibition does not select for resistance against the anti-biofilm effect. A dose-response curve was determined demonstrating the effect of treatment of wild-type (WT) *Salmonella* Typhimurium ATCC14028 cultures with the 2-AI-based EPS inhibitor RC41 on both the planktonic biomass (•) and biofilm biomass (▪) (**A**). Optical Density (OD) values were determined after 48 h of incubation and normalized relative to an untreated control (0 μM) as a reference (horizontal dashed line). A concentration of 50 μM (vertical dashed line) was selected for long-term treatment since, at this concentration, no inhibition of planktonic biomass was observed (**B**), while biofilm biomass was substantially reduced (**C**, ±75% inhibition). Next, three independent *Salmonella* biofilms were treated for 20 two-day cycles with either 50 μM of RC41 (RC41-evolved lineages) or with 0 μM (control-evolved lineages). After this long-term treatment, the susceptibility to RC41-mediated biofilm inhibition of the evolved populations was quantified and compared to the susceptibility of wild-type *Salmonella* (**D**). Hereto, populations were treated with 50 μM of RC41, and both planktonic biomass (**E**) and biofilm biomass (**F**) were quantified after 48 h of incubation. Based on these results, percentual biofilm biomass inhibition was calculated relative to untreated (0 μM) control samples. For wild-type *Salmonella*, each datapoint represents a biological repeat ($n = 5$). For the evolved populations, each datapoint represents an independently evolved lineage, for which the average of five replicates is shown ($n = 3$). Bars represent the mean, and error bars represent the standard deviation. Significance was tested using a paired, two-tailed Student's *t*-test (**B**, **C**) or an ordinary one-way ANOVA, followed by Tukey's multiple comparisons test (**D**–**F**). All *p*-values are shown.

likely result in a σ^S loss-of-function. In lineage 1, on the other hand, three mutations (Leu363Pro, His450Tyr, Arg481Cys) in the *rpoC* gene encoding the β' subunit of the RNAP complex were found. Intriguingly, all three amino acid substitutions map to the exact location where ppGpp binds the RNAP (Fig. 2E)[33]. Guanosine tetraphosphate (ppGpp) acts as an alarmone that, in response to nutrient starvation, binds the RNAP. The binding of ppGpp then decreases the affinity of the RNAP to recruit the household sigma factor σ^{70}, favoring binding to alternative stress-related sigma factors such as σ^S instead[34]. Based on the *rpoS* mutations observed in the other two lineages, we hypothesize that the *rpoC* mutations disrupt the ppGpp binding pocket, reducing the affinity of the RNAP for σ^S and, hence, decreasing the expression of the σ^S regulon in an indirect fashion. No mutations in *ramR* or the RNAP were found in the control-evolved populations, suggesting that they are specifically selected for by treatment with the EPS inhibitor.

Given the high abundance of both efflux- and polymerase-related mutations observed in the treated populations, we also sequenced three additional *Salmonella* biofilms that were previously exposed to RC41 treatment (Supplementary Data)[7]. While *ramR* mutations were only found in low frequencies (<1%) in these populations, other efflux-related mutations occurred with higher frequencies. For example, a 12-nucleotide deletion in the promoter of *marA*, which functions as a transcriptional activator of the AcrAB efflux pump, was the most frequent mutation observed in one of these lineages. Even more remarkable, all three populations also contained RNAP mutations that either map to *rpoS* (Val103fs, Trp149Leu and Gln257fs) or the ppGpp binding pocket (*rpoC*: His419Pro; *rpoZ*: Arg3del, Arg3_Gln6del, Ala24fs) (Supplementary Fig. 3). Taken together, these observations indicate that treatment with the 2-AI-based EPS inhibitor RC41 selects for mutations related to the AcrAB efflux pump and the RNAP.

Table 1 | Genotypic changes in *Salmonella* biofilms after long-term treatment with a 2-AI-based EPS inhibitor

RC41-evolved population	GeneID	Mutation frequency	Position in genome (NC_016856)	Reference nucleotide	Alternative nucleotide	Protein change
Lineage 1	STM14_RS03505 (= *ramR*)	35%	639541	T	A	Upstream
		14%	639548	T	C	Upstream
	Intergenic region	35%	2126855	G	A	/
	STM14_RS21825 (= *rpoC*)	29%	4384681	T	C	Leu363Pro
		25%	4384941	C	T	His450Tyr
		21%	4385034	C	T	Arg481Cys
	STM14_RS25180	10%	2782419	A	AGCAAGG	Upstream
Lineage 2	STM14_RS03505 (= *ramR*)	70%	638867	C	T	Trp185*
		24%	639274	T	G	Thr50Pro
	STM14_RS12350 (= *yejM*)	35%	2381116	G	A	Arg215Gln
	STM14_RS09440 (= *lapB*)	15%	1812470	GAGCTGCGTC	G	Asp299_Ala301del
	STM14_RS15660 (= *rpoS*)	11%	3086606	GGTCGTTAT	G	Asp37fs
Lineage 3	STM14_RS03505 (= *ramR*)	100%	639249	A	C	Leu58Trp
	STM14_RS11805 (= *asmA*)	23%	2256692	C	T	Trp570*
		12%	2256669	G	A	Gln578*
	STM14_RS15660 (= *rpoS*)	18%	3086279	A	G	Trp149Arg
		16%	3086606	GGTCGTTAT	G	Asp37fs

Salmonella Typhimurium ATCC14028 biofilms were treated with the 2-AI-based EPS inhibitor RC41 for 40 days, after which end-point biofilm populations were subjected to whole-genome sequencing. Only mutations occurring with a frequency of ≥10% in the 2-AI-treated biofilms and <1% in the parental strain and control-evolved biofilms were included, as these mutations are believed to be specifically selected for by 2-AI treatment. The full list of identified mutations can be found in Supplementary Data.
The '*' indicates a mutation of the indicated amino acid into a premature stop codon.

Long-term treatment with an EPS inhibitor results in a decreased biofilm-forming capacity and elevated efflux levels

After establishing that long-term treatment with the EPS inhibitor influenced the evolutionary outcome by selecting for mutations related to the AcrAB efflux pump and the RNAP without selecting for resistance against the anti-biofilm effect, the phenotypic consequences of these adaptations were further explored. We first evaluated the ability of the evolved populations to produce a biofilm in the absence of any EPS inhibitor (Fig. 3). While no statistically significant differences were observed, we did observe a trend towards a reduction in biofilm biomass for the RC41-evolved populations (0.23 OD_{570nm}) compared to both the control-evolved (0.36 OD_{570nm}) and wild-type (0.38 OD_{570nm}) *Salmonella* populations (Fig. 3A). Moreover, when we screened the biofilm-forming capacity of individual clones isolated from the RC41-evolved populations (six per population), they indeed produced significantly less biofilm biomass compared to wild-type *Salmonella* clones (Supplementary Fig. 2). This also corresponded with a significant increase in planktonic biomass in the system compared to both control groups (Fig. 3B), further confirming a shift from biofilm growth to planktonic growth in the RC41-evolved populations. The RC41-evolved populations, but not the control populations, also exhibited a reduced expression of the central biofilm regulator *csgD* (Fig. 3C). This observation suggests that the reduced biofilm formation could be due to the mutations in the RNAP, as the *csgD* gene is part of the σ^S regulon[35]. To further explore this hypothesis, we randomly picked 20 clones from each evolved population and qualitatively assessed functionality of the σ^S regulon using a catalase assay. The *Salmonella* catalase (*katE*) is regulated by σ^S and is, therefore, frequently used as a rapid read-out for expression of the σ^S regulon[36]. Between 5% and 20% of the tested clones failed to show catalase activity, which roughly corresponds with the observed frequencies of *rpoS* and *rpoC* mutations in each population (Supplementary Table 2). For the clones that did not show catalase activity, the *rpoS* and *rpoC* genes were amplified and Sanger sequenced. As expected, 7 out of 8 catalase-negative clones contained at least one of the listed mutations (Table 1) in either *rpoS* or *rpoC*, further supporting that these mutations are responsible for a reduced expression of the σ^S regulon.

Since, in addition to the RNAP mutations, all RC41-evolved populations contained mutations in *ramR*, a known repressor of the AcrAB efflux pump, the average efflux activity across the evolved populations was also quantified and compared to wild-type efflux levels using a Nile Red assay (Fig. 4A–C). On average, the RC41-evolved populations showed a faster drop in fluorescence compared to both the control-evolved populations and wild-type *Salmonella*, indicating faster efflux of the periplasmic Nile Red dye (Fig. 4A). To quantitatively compare efflux levels, an exponential one-phase decay model was fitted, and the fluorescence half-life (s) and rate constant (K, s^{-1}) were estimated[37]. While we observed a clear trend towards elevated efflux levels for the RC41-evolved populations, the averages were not statistically significant (Fig. 4B, C). However, when the half-life and rate constants were determined separately for each population, the RC41-evolved populations 2 and 3 both showed a significant increase in efflux, resembling the efflux increase observed in a *ramR* deletion construct (Δ*ramR*) (Supplementary Fig. 4). This suggests that the *ramR* mutations observed in these two RC41-evolved populations (Trp185*, Thr50Pro, Leu58Trp) at least partially compromise the ability of *ramR* to repress expression of the *acrAB* efflux pump, hence resulting in increased efflux. Interestingly, we did not observe a significant increase in the efflux rate for the RC41-evolved population 1. Possibly, we were unable to detect an increase in efflux in our population-level measurement because of the relatively lower frequency of *ramR* mutations (±35%) in this lineage compared to the other two lineages (≥70%).

Given the observed increase in efflux for two of the RC41-evolved populations, it was evaluated whether this also translated to increased resistance levels against clinically relevant antibiotics. For this reason, the Minimal Inhibitory Concentration (MIC) of the evolved *Salmonella* populations was determined against azithromycin, ciprofloxacin, and meropenem (Fig. 4D–F). Both azithromycin (Fig. 4D) and ciprofloxacin (Fig. 4E) have an intracellular mode of action, and overexpression of the AcrAB efflux pump or mutations in the *ramR* gene have previously been

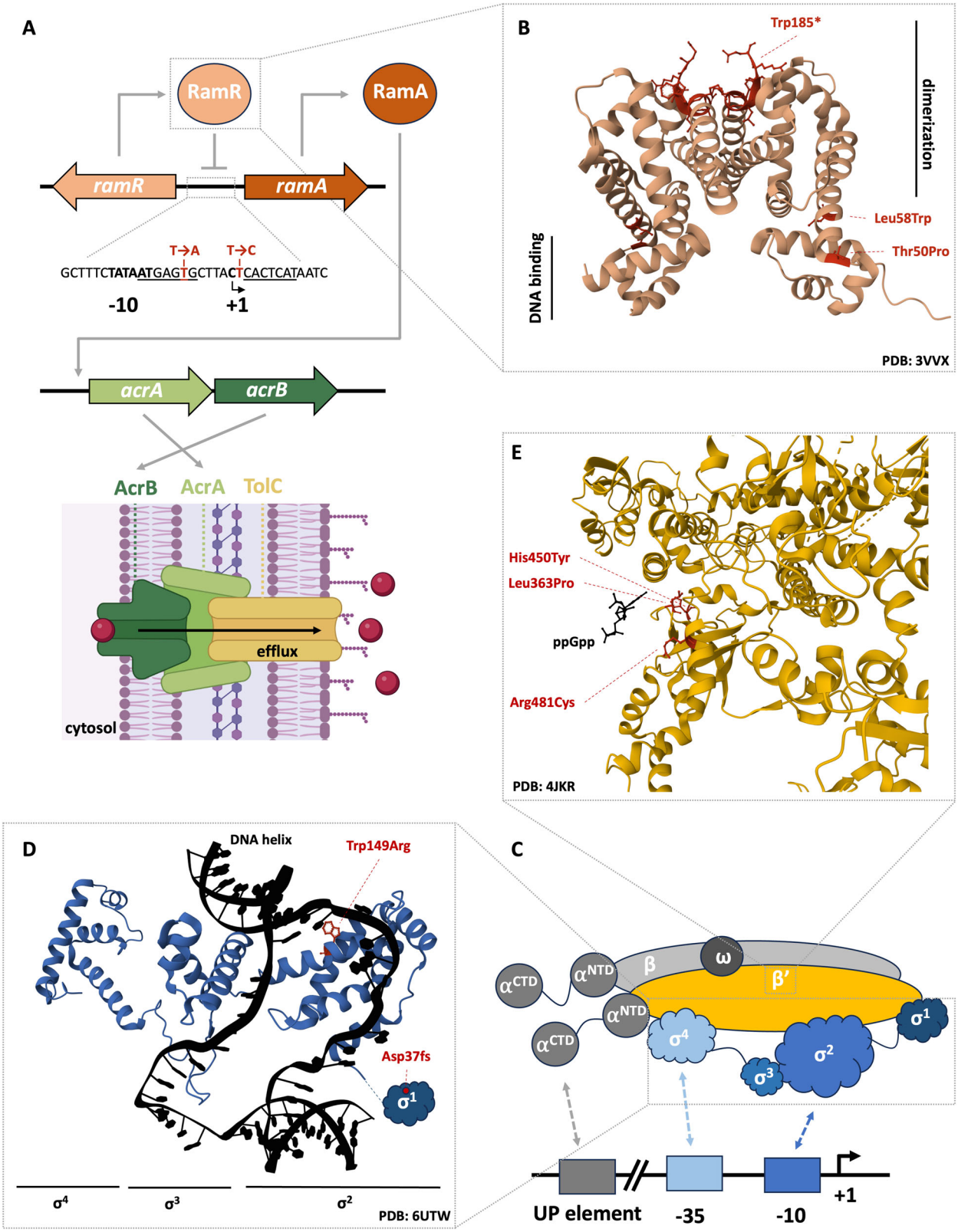

shown to render *Salmonella* more resistant toward these antibiotics. We also included meropenem (Fig. 4F), a cell-wall synthesis inhibitor[38], as enhanced efflux is not expected to increase resistance to this antibiotic[39]. In agreement with the observed increase in efflux levels, the RC41-evolved populations showed higher MICs for azithromycin and ciprofloxacin but not for meropenem. Moreover, the Δ*ramR* strain showed highly similar trends as the RC41-evolved populations. Interestingly, we observed elevated MICs for all three RC41-evolved populations, also for lineage 1 for which we did not detect a substantial increase in efflux. This further supports the idea that the *ramR* mutations in this population also increase efflux levels, but we did not detect this in the Nile Red assay due to the limited frequency of these mutations in the population. In contrast to the Nile Red assay, lower

Fig. 2 | Long-term treatment with an EPS inhibitor selects for mutations related to efflux pumps and the RNA polymerase. During 40 days of treatment with the 2-AI-based EPS inhibitor RC41, all three independently evolved *Salmonella* Typhimurium ATCC14028 biofilms accumulated mutations associated with the transcriptional regulator RamR, which functions as a repressor of RamA, a transcriptional activator of the AcrAB efflux pump (**A**). These mutations map either to the RamR binding site (inverted repeats are underscored), the dimerization interface (Trp185*), or the DNA binding region (Thr50Pro, Leu58Trp) (**B**). The *S.* Typhimurium RamR crystal structure was retrieved from PDB 3VVX[60]. In addition to ramR mutations, all three independently evolved *Salmonella* biofilms also accumulated mutations in different subunits of the RNA polymerase complex (**C**). In two lineages, these mutations (Asp37fs, Trp149Arg) map to *rpoS*, which encodes the stationary phase sigma factor σ^S (**D**). The *Escherichia coli* σ^S crystal structure was retrieved from PDB 6UTW[61]. In the remaining lineage, mutations (Leu363Pro, His450Tyr, Arg481Cys) are observed in *rpoC*, which encodes the β' subunit of the RNA polymerase complex. These mutations all map to the ppGpp binding pocket (**E**). The crystal structure of the *E. coli* RNA polymerase in complex with ppGpp was retrieved from PDB 4JKR[33]. No *ramR* or RNA polymerase mutations were observed in wild-type biofilms or control biofilms evolved under similar conditions but without RC41 treatment.

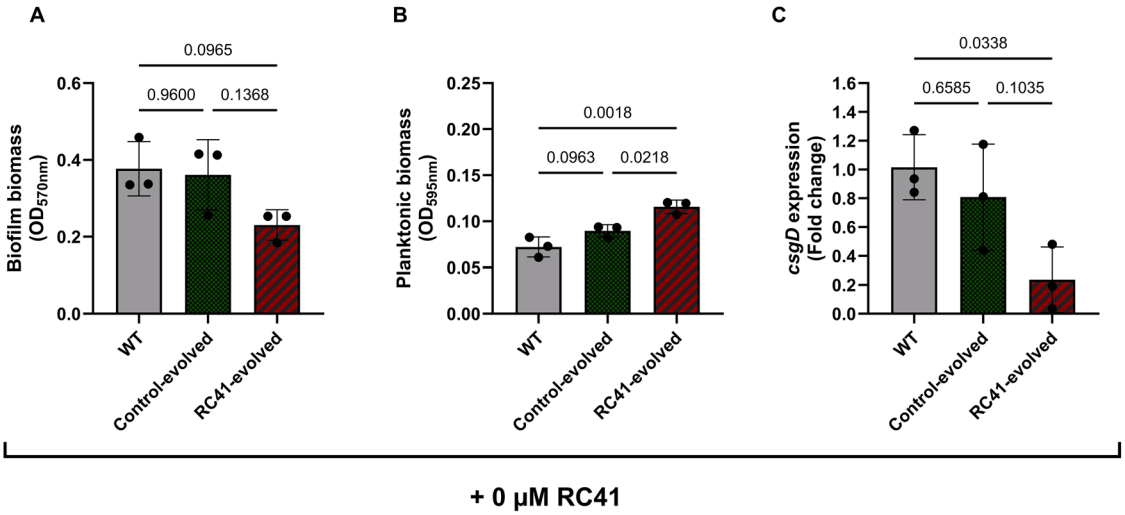

Fig. 3 | Long-term treatment with an EPS inhibitor selects for reduced biofilm formation and *csgD* expression. Biofilm biomass (**A**) and planktonic biomass (**B**) of the evolved *Salmonella* Typhimurium ATCC14028 populations were quantified after 48 h in the absence of any EPS inhibitor and compared to wild-type (WT) biomass levels. To further investigate the trend towards a reduction in biofilm biomass in the RC41-evolved lineages, population-level *csgD* expression was quantified in 48 h biofilms for both wild-type and evolved populations using an RT-qPCR (**C**). For each sample, the fold change in normalized *csgD* expression was calculated relative to the wild-type samples using the ΔΔCt method. For wild-type *Salmonella*, each datapoint represents a biological repeat ($n = 3$). For the evolved populations, each datapoint represents an independently evolved lineage, for which the average of three replicates is shown ($n = 3$). Bars represent the mean, and error bars represent the standard deviation. Significance was tested using an ordinary one-way ANOVA, followed by Tukey's multiple comparisons test. All *p*-values are shown.

mutation frequencies are likely less important in MIC assays, as even rare mutations can take over the population and allow growth during antibiotic exposure.

Evolved populations have adapted to overcome an unintended growth delay

We subsequently aimed to better understand why mutations related to the AcrAB efflux pump were selected upon exposure to the EPS inhibitor. This was not due to direct effects of RC41 on this efflux pump as short-term RC41 treatment did not substantially impact the efflux of Nile Red (Supplementary Fig. 5). Since we observed that higher concentrations of RC41 inhibited planktonic biomass after 48 h (Fig. 1), we first investigated potential toxic side effects of RC41 on planktonic growth in more detail by following the growth of wild-type *Salmonella* over time in the absence and presence of 50 µM of the EPS inhibitor (Fig. 5A). From these growth curves, a clear delay in growth was observed in the cultures treated with RC41. To quantify bacterial growth rates (Fig. 5B) and lag times (Fig. 5C), a Zwietering-modified Gompertz model was used to fit the experimentally obtained growth curves[40]. This analysis confirms that RC41 treatment significantly decreases the growth rate (0.026 OD_{600nm} h^{-1}) and increases the lag time (5.35 h) compared to untreated *Salmonella* cultures (0.045 OD_{600nm} h^{-1}; 3.44 h). These findings demonstrate that in addition to inhibiting EPS production and biofilm formation, RC41 treatment also causes an unintentional growth delay. Interestingly, despite the delayed growth, end-point optical densities of treated cultures were substantially higher than for the untreated cultures, for which we observed a distinct drop in the growth curves around the onset of the stationary phase. This drop is likely caused by aggregation, as our experimental conditions (i.e., 1:20 TSB & 25 °C) were selected to promote biofilm formation of *Salmonella*. The drop in density was not observed for the cultures treated with RC41, which agrees with an inhibition of EPS production and, thus, biofilm formation and aggregation.

Since cells that are able to overcome the RC41-mediated growth delay would experience a fitness advantage, we expected that this growth delay imposed a selection pressure during our evolution experiment. To evaluate this hypothesis, growth curves were also analyzed for the evolved populations (Fig. 5A; Supplementary Fig. 6). In the absence of RC41 treatment, growth curves of the evolved populations were almost identical to wild-type *Salmonella* (Supplementary Fig. 6). In the presence of RC41 treatment, however, growth rates of the RC41-evolved populations (0.034 OD_{600nm} h^{-1}) were significantly higher compared to both wild-type (0.022 OD_{600nm} h^{-1}) and control-evolved populations (0.021 OD_{600nm} h^{-1}) (Fig. 5B; Supplementary Table 3). Moreover, the RC41-evolved populations almost completely overcame the RC41-mediated growth inhibition, as growth rates in the presence (0.034 OD_{600nm} h^{-1}) and absence (0.037 OD_{600nm} h^{-1}) of RC41 treatment were almost identical. In contrast, the growth rate of both wild-type and control-evolved populations remained strongly reduced during RC41 exposure. Additionally, in the presence of RC41 treatment, lag times of the RC41-evolved populations (3.66 h) were significantly reduced compared to both wild-type (5.28 h) and control-evolved populations (5.59 h) (Fig. 5C; Supplementary Table 4). Together,

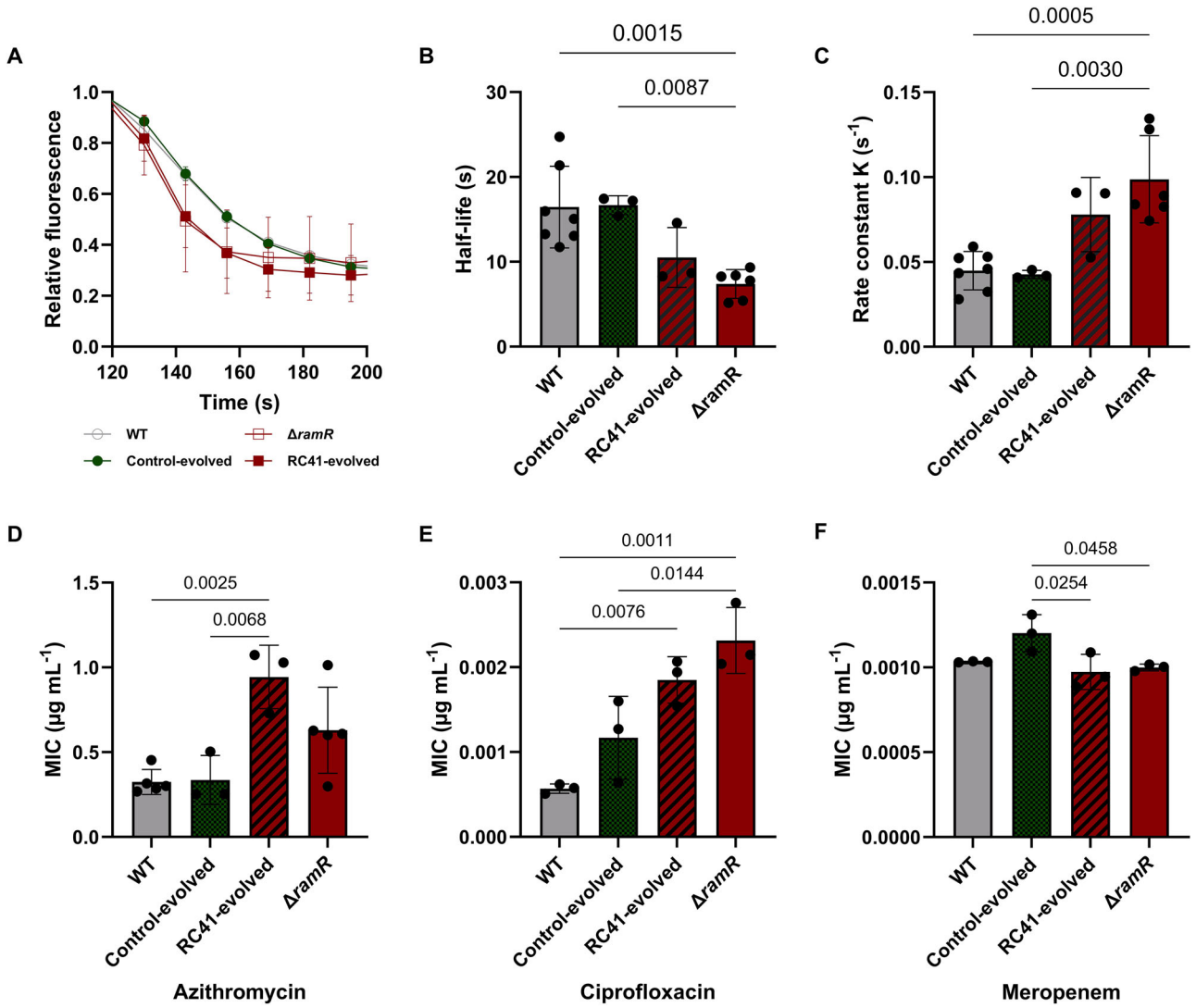

Fig. 4 | Long-term anti-biofilm treatment selects for increased efflux, which reduces susceptibility to certain antibiotics. Efflux of the evolved *Salmonella* Typhimurium ATCC14028 populations was quantified by measuring the decay in fluorescence of cells loaded with the periplasmic dye Nile Red (**A**). A one-step exponential decay model was fit, and the half-life (**B**) and rate constant (K; **C**) of the fluorescent decay were estimated. In Supplementary Fig. 4, the half-life and rate constant for each individual population can be found. To evaluate whether the observed increase in efflux for the RC41-evolved populations also corresponded to decreased susceptibility against clinically relevant antibiotics, Minimal Inhibitory Concentration (MIC) values against azithromycin (**D**), ciprofloxacin (**E**), and meropenem (**F**) were determined. Wild-type (WT) *S.* Typhimurium and an isogenic *ramR* deletion construct (Δ*ramR*) were included as references. For these strains, each datapoint represents a biological repeat ($n = 3$–7). For the evolved populations, each datapoint represents an independently evolved lineage, for which the average of three to eight replicates is shown ($n = 3$). Bars represent the mean, and error bars represent the standard deviation. For the relative fluorescence vs time graph, each datapoint represents an average value, and standard deviations are shown as error bars. Significance was tested using an ordinary one-way ANOVA, followed by Tukey's multiple comparison test. For all significant differences, *p*-values are shown.

these results demonstrate that the RC41-evolved populations, but not the control-evolved populations, have adapted to overcome the growth delay imposed by EPS inhibitor treatment.

To investigate whether this effect could be linked to an increase in efflux levels, growth curves were also analyzed for a *ramR* deletion strain (Δ*ramR*) (Fig. 5). Visual inspection of the growth curves and the extracted growth parameters both show a trend towards faster growth of the Δ*ramR* strain compared to the wild-type and control-evolved populations under RC41 treatment, but not in the absence of the EPS inhibitor. This provides an indication that *ramR* loss-of-function and the concomitant increase in efflux might confer a growth advantage, specifically during RC41 exposure. Despite the observed trends, the Δ*ramR* strain still grows substantially slower compared to the RC41-evolved populations. Based on these results, it can be concluded that a *ramR* loss-of-function by itself is only able to partially overcome the RC41-mediated growth delay. Since we also observed *rpoS* mutations in the RC41-evolved populations, we also evaluated the growth of a Δ*rpoS* strain and a Δ*ramR*Δ*rpoS* double-deletion mutant, mimicking the sequential selection of both mutations. Comparable to the Δ*ramR* strain, we observed a trend towards an increased growth rate of the Δ*rpoS* strain (0.032 OD_{600nm} h^{-1}) compared to the wild-type (0.022 OD_{600nm} h^{-1}) during RC41 exposure. In contrast, the lag time of the Δ*rpoS* mutant (6.17 h) was elongated by almost an hour compared to the wild-type (5.28 h). This indicates that while *rpoS* loss-of-function might partially compensate for the delay in growth rate imposed by RC41 treatment, it becomes even more susceptible to the increased lag time. Moreover, a Δ*ramR*Δ*rpoS* double deletion construct showed similar growth characteristics (0.028 OD_{600nm} h^{-1}; 4.93 h) compared to the Δ*ramR* single deletion (0.027 OD_{600nm} h^{-1}; 4.62 h), indicating that *rpoS* loss-of-function in a Δ*ramR* background does not further improve growth under RC41 treatment. It should be noted, however, that both the Δ*rpoS* and Δ*ramR*Δ*rpoS*

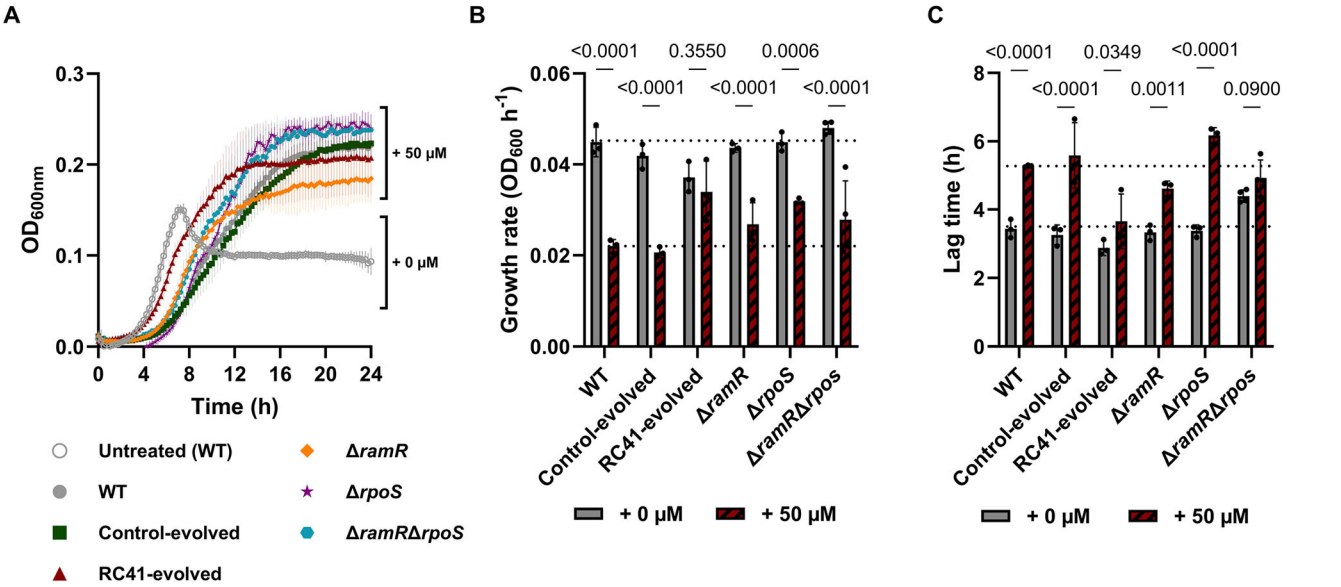

Fig. 5 | RC41-evolved populations have adapted to overcome an unintended growth delay caused by EPS inhibitor treatment. Planktonic growth of wild-type (WT) *Salmonella* Typhimurium ATCC14028 and end-point evolved populations was measured in the presence or absence of 50 µM of the 2-AI-based EPS inhibitor (RC41). **A** *ramR* and *rpoS* deletion construct (Δ*ramR* & Δ*rpoS*) and a double deletion construct (Δ*ramR*Δ*rpoS*) were included as references. Except for the wild-type, only growth curves for treated (50 µM) samples are shown. Growth curves for the untreated samples can be found in Supplementary Fig. 6. Growth rates (OD_{600nm} h^{-1}; **B**) and lag times (h; **C**) were extracted from growth curves by fitting a Zwietering-modified Gompertz model. Horizontal dashed lines indicate the wild-type growth parameters for reference. For the wild-type, Δ*ramR*, Δ*rpoS*, and Δ*ramR*Δ*rpoS* strains, each datapoint represents a biological repeat ($n = 3–4$). For the evolved populations, each datapoint represents an independently evolved lineage, for which the average of three replicates is shown ($n = 3$). Lines and bars represent the mean, and error bars represent the standard deviation. Significance was tested using a two-way ANOVA, followed by Tukey's multiple comparisons test. All *p*-values can be found in Supplementary Tables 3 and 4.

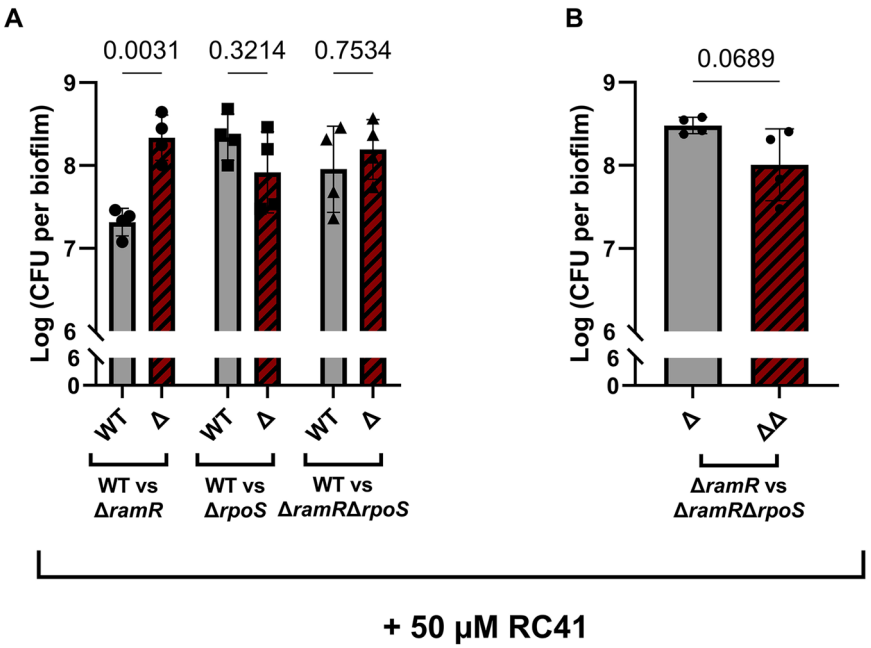

Fig. 6 | *ramR*, but not *rpoS* loss-of-function, provides a fitness advantage in biofilms treated with the EPS inhibitor. Biofilm competition experiments in small Petri dishes were performed between wild-type (WT) *Salmonella* Typhimurium ATCC14028 and isogenic deletion constructs (Δ*ramR*, Δ*rpoS*, Δ*ramR*Δ*rpoS*) (**A**), or between the Δ*ramR* and Δ*ramR*Δ*rpoS* construct (**B**). Biofilms were inoculated in a 1:1 ratio and treated with 50 µM of the 2-AI-based EPS inhibitor RC41. After 48 h of incubation, biofilms were scraped off, and both competitors were quantified by counting Colony Forming Units (CFU). Each datapoint represents a biological repeat ($n = 4$). Bars represent the mean, while error bars represent the standard deviation. Significant differences in cell counts between both competitors were tested using a two-way ANOVA, followed by Sidak's multiple comparisons test (**A**) or a paired, two-tailed Student's *t*-test (**B**). All *p*-values are shown.

strains showed an extended exponential growth phase and a delayed onset of the stationary phase, resulting in higher end-point yields compared to the wild-type strain.

Enhanced efflux increases fitness during EPS inhibitor treatment

To further elucidate whether enhanced efflux provides a fitness advantage in *Salmonella* biofilms treated with the EPS inhibitor, biofilm competition experiments were carried out (Fig. 6A). In these experiments, wild-type *Salmonella* and isogenic Δ*ramR* cells were inoculated in a 1:1 ratio. After static incubation for 48 h, biofilms were scraped off, and cell counts of both strains were determined by plate counting. To distinguish between wild-type and Δ*ramR* cells, the wild-type strain constitutively expressed a green fluorescent protein (*gfpmut3*), whereas the Δ*ramR* cells produced a red fluorescent protein (*dsRed.T4*). We have previously demonstrated that these fluorescent markers do not affect the outcome of competition and can be used interchangeably in this biofilm setup[7]. In line with the trend observed

in the growth curves, the Δ*ramR* strain strongly outcompeted the wild-type strain when biofilms were grown in the presence of RC41 (Fig. 6A). After a single growth cycle, biofilms inoculated in a 1:1 ratio consisted of approximately 90% of the Δ*ramR* mutant. This demonstrates that enhanced efflux due to a *ramR* deletion confers a substantial fitness advantage during treatment with RC41 in our biofilm setup and could explain why *ramR* mutations were selected during the evolution experiment. In contrast, the Δ*ramR* strain was unable to significantly outcompete the wild-type strain in control experiments where biofilms were only treated with the carrier solvent (DMSO) (Supplementary Fig. 7). This confirms that the benefit obtained from *ramR* loss-of-function is specific to the presence of RC41, which is also in line with the observation that no efflux-related mutations were selected in the control-evolved lineages.

In contrast to the Δ*ramR* strain, an *rpoS* loss-of-function (Δ*rpoS*) strain was unable to outcompete the wild-type in either treated or untreated biofilms (Fig. 6; Supplementary Fig. 7). On average, Δ*rpoS* cells even seemed to perform slightly worse compared to the wild-type in the presence of RC41, and their fraction in the biofilm was reduced to approximately 30% after 48 h. Also when the *rpoS* loss-of-function was introduced into a Δ*ramR* background, mimicking a sequential selection of both mutations, the resulting Δ*ramR*Δ*rpoS* double deletion construct was unable to significantly outcompete either the wild-type strain (Fig. 6A) or the single Δ*ramR* deletion (Fig. 6B). This is in agreement with the growth analysis and indicates that, under the selected experimental conditions, *rpoS* loss-of-function does not seem to provide a fitness benefit, even though *rpoS* mutations appeared in multiple independently evolved lineages during RC41 treatment. This discrepancy could potentially be explained by distinct fitness effects of the *rpoS* deletion mutant versus the evolved *rpoS* mutations.

Chemical modification of the EPS inhibitor partially alleviates the unintended growth effects

To prevent the selection of mutants with increased efflux and concomitant cross-resistance to antibiotics, we sought to overcome the unintended growth delay while retaining the anti-biofilm activity. It was first explored whether lower concentrations of the RC41 molecule still delayed growth by analyzing planktonic growth curves (Supplementary Fig. 8). Even concentrations as low as 20 μM still almost halved the *Salmonella* growth rate (0.024 OD_{600nm} h^{-1}) and increased the lag time (6.24 h) by over two hours compared to untreated cultures (0.040 OD_{600nm} h^{-1}; 3.61 h). At concentrations lower than 20 μM, no biofilm biomass inhibition can be observed anymore (Fig. 1A). Consequently, the growth defect of these concentrations of the EPS inhibitor was not evaluated. These results indicate that reducing the RC41 concentration used for treatment is not a viable solution to prevent selection for increased efflux, as the anti-biofilm effect and the unintended growth defect cannot be uncoupled.

As an alternative strategy, it was explored whether chemical modification of the EPS inhibitor could increase its specificity by reducing the growth defect without losing the anti-biofilm activity. Based on structure-activity insights acquired during other projects, the N-cyclopentyl chain of RC41 was replaced with an N-octylamine group, and the 5-(4-chlorophenyl) chain was substituted for a 5-(4-bromophenyl) chain (Supplementary Fig. 1B). To validate that the modified 2-AI-based EPS inhibitor, i.e., N-octylamine-5-(4-bromophenyl)-1H-imidazol-2-amine (RC6), retained its anti-biofilm activity, a dose-response curve was determined (Fig. 7A). Similar to RC41, a dose-dependent inhibition of biofilm biomass was observed. However, while RC41 only started inhibiting biofilm biomass at concentrations above 20 μM, RC6 already showed a significant inhibition (>50%) at a concentration of only 8 μM (Fig. 7B), demonstrating that RC6 possesses even more potent anti-biofilm activity compared to RC41. For concentrations above 25 μM, complete inhibition (>99%) of biofilm biomass was observed. Again, higher concentrations (≥50 μM) also inhibited planktonic biomass, indicating that RC6 also has unintended side effects on planktonic growth at elevated concentrations.

Based on the dose-response curve, a concentration range of 5–20 μM of RC6 was selected to further evaluate growth defects by analyzing planktonic growth curves (Fig. 7D). Only at a concentration of 20 μM, a significant reduction in growth rate (0.025 OD_{600nm} h^{-1}) was observed compared to untreated cultures (0.038 OD_{600nm} h^{-1}). This reduction in growth rate was comparable to the reduction observed for cultures treated with 50 μM of RC41 (0.026 OD_{600nm} h^{-1}; Fig. 5). At lower RC6 concentrations, no reductions in growth rate were observed (Fig. 7E). Despite the limited effects on growth rate, a dose-dependent increase in lag time was still observed starting from concentrations as low as 10 μM (Fig. 7F). Taken together, these results demonstrate that the chemically modified EPS inhibitor shows even more potent anti-biofilm activity against *Salmonella*, while the unintended growth defect is reduced but not completely eliminated. Since a concentration of 10 μM inhibited biofilm biomass by over 50% while not reducing the growth rate, it was further explored whether these conditions still selected for increased efflux through *ramR* loss-of-functions. Hereto, short-term biofilm competition experiments between wild-type *Salmonella* and the *ramR* deletion construct (Δ*ramR*) were performed (Fig. 7C). In contrast to the results obtained in biofilms treated with RC41, the Δ*ramR* strain was no longer able to outcompete the wild-type when biofilms were treated with 10 μM RC6. Under these conditions, the Δ*ramR* strain retained its initial frequency of approximately 50%, indicating that *ramR* loss-of-function is selection-neutral. Based on these results, *ramR* loss-of-function and the accompanying increase in efflux do not seem to provide a selective advantage during treatment with 10 μM of RC6.

Discussion

Anti-biofilm molecules have emerged as a promising anti-virulence strategy with potential for both industrial and clinical applications[41]. Despite encouraging results, the long-term evolutionary consequences of EPS inhibition in bacterial populations remain largely unexplored. To address this, we subjected *Salmonella* biofilms to 40 days of treatment with 5-(4-chlorophenyl)-N-cyclopentyl-1H-imidazol-2-amine (RC41), a well-characterized 2-AI-based EPS inhibitor. Consistent with our previous findings[7], no resistance to the anti-biofilm effect of RC41 developed, and even after long-term treatment, *Salmonella* populations remained as susceptible to EPS inhibition as the untreated parental populations (Fig. 1). However, unintended side effects on private traits could undermine the evolutionary robustness of public good inhibitors. In such cases, a selection pressure is applied on the cell to become resistant to this side effect, resulting in a fitness increase compared to the non-resistant cells. This has previously been observed with flucytosine and C-30. Flucytosine is an anti-virulence drug that inhibits the production of pyoverdine, a public siderophore of *Pseudomonas aeruginosa*[42]. While flucytosine effectively suppresses pyoverdine production, it also delays planktonic growth. As a result, *P. aeruginosa* populations experimentally evolved with the siderophore inhibitor adapted to overcome the growth delay by acquiring loss-of-function mutations in the *upp* gene, encoding a uracil phosphoribosyl-transferase required for intracellular activation of flucytosine. Consequently, the adapted populations also acquired resistance to the anti-virulence effect, resulting in a full restoration of siderophore production under drug treatment. Similar observations have been made for C-30, a synthetic furanone that interferes with quorum sensing in *P. aeruginosa*[43]. While this quorum-sensing inhibitor did not inhibit planktonic growth in nutrient-rich media, a significant biomass reduction was observed under nutrient-limiting conditions. In response, populations repeatedly treated with C-30 acquired mutations in *mexR* or *nalC*, resulting in upregulated efflux activity. In turn, this compensated for the growth inhibition, concomitantly also conferring resistance to the inhibition of quorum sensing. These examples highlight the importance of minimizing unintended side effects when designing public good inhibitors, as such effects can drive adaptive responses that compromise the inhibitor's evolutionary robustness.

Analogous to the examples discussed above, we discovered that RC41 treatment also unintentionally delays *Salmonella* growth in addition to the targeted EPS inhibition (Fig. 5). It has been reported that other 2-AI-based chemicals can interfere with the electron transport chain in *Mycobacterium tuberculosis*, thus collapsing the proton motive force and depleting

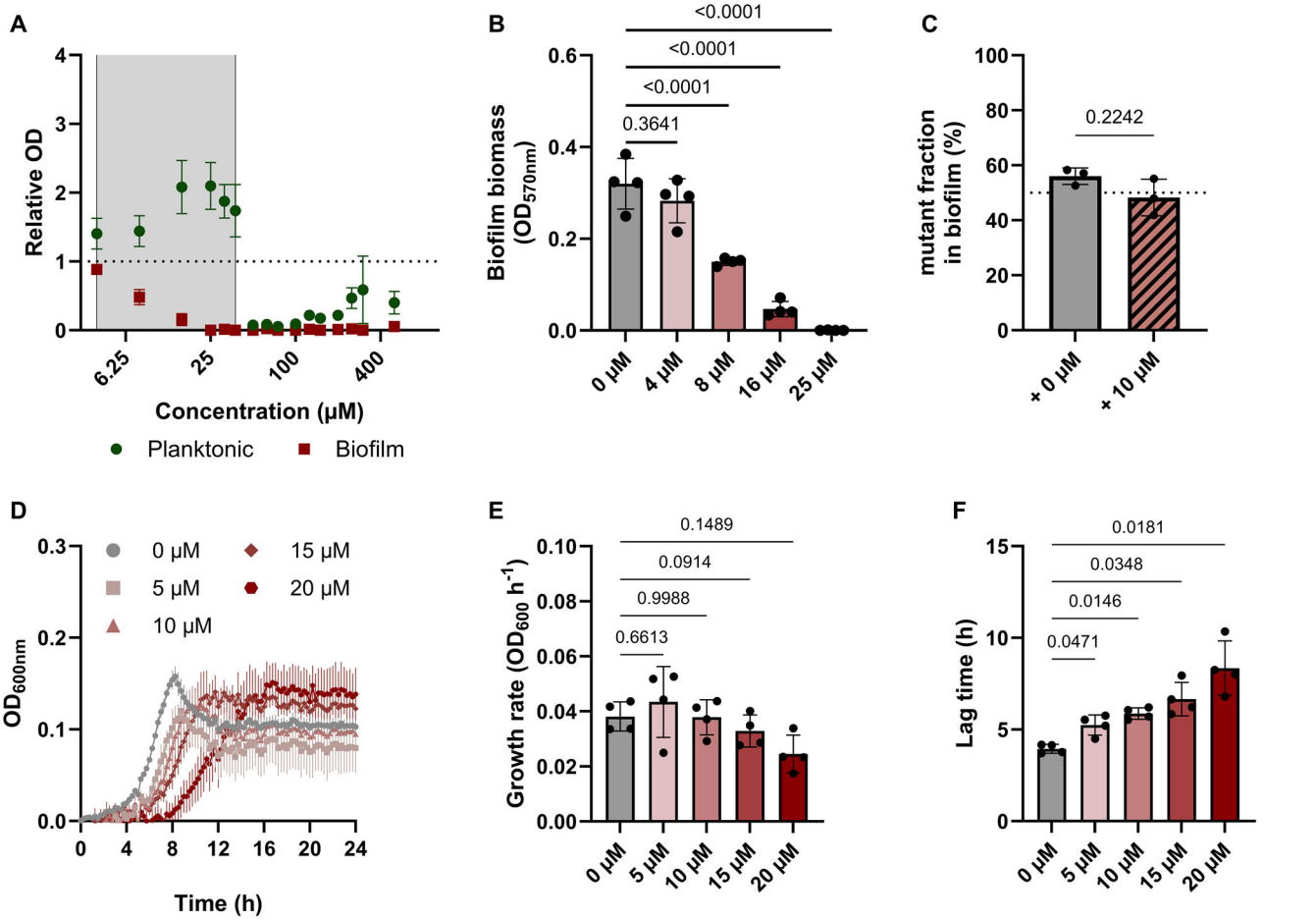

Fig. 7 | Effect of RC6 treatment on planktonic and biofilm growth of *Salmonella*. Dose-response curve (**A**, **B**) demonstrating the effect of treatment of *Salmonella* Typhimurium ATCC14028 cultures with the 2-AI-based EPS inhibitor RC6 on both the planktonic biomass (•) and biofilm biomass (▪) after 48 h of incubation. Optical Density (OD) values were normalized relative to an untreated control (0 μM) as a reference (horizontal dashed line). From a concentration of 4 to 38 μM (shaded in gray), a dose-dependent inhibition of biofilm biomass was observed without inhibition of planktonic biomass. In addition to end-point measurements, planktonic growth was measured over time in the presence of RC6 (0 μM–20 μM) to evaluate unintended growth effects (**D**). Growth rates (OD_{600nm} h^{-1}; **E**) and lag times (h; **F**) were extracted from growth curves by fitting a Zwietering-modified Gompertz model. Based on these results, a concentration of 10 μM was selected to perform biofilm competition experiments in small Petri dishes between wild-type *Salmonella* and an isogenic *ramR* deletion construct (Δ*ramR*) (**C**). Biofilms were inoculated in a 1:1 ratio and treated with 10 μM of RC6. After 48 h of incubation, biofilms were scraped off, and both competitors were quantified by counting Colony Forming Units (CFU). Each datapoint represents a biological repeat ($n = 3–4$). Bars represent the mean, while error bars represent the standard deviation. In (**B**), (**E**), and (**F**), the significance between the treated and untreated groups was tested using an RM one-way ANOVA, followed by Dunnett's multiple comparisons test. In (**C**), significant differences in cell counts between both competitors were tested using a paired, two-tailed Student's *t*-test. All *p*-values are shown.

intracellular ATP levels[44]. It is possible that such a disruption of energy homeostasis explains the observed growth delay in *Salmonella*, but additional research is required to further investigate the underlying mechanism. Intriguingly, while we did not observe any resistance to the anti-biofilm effect after long-term treatment with RC41 (Fig. 1), *Salmonella* biofilms did adapt to overcome the unintended growth delay imposed by anti-virulence treatment (Fig. 5). This observation demonstrates that the unintended growth delay is not essential for the anti-biofilm activity of RC41, and that both effects are at least partially uncoupled. Moreover, this indicates that unintended side effects of public good inhibitors are not always detrimental to their evolutionarily robust character, as it seems to be possible for bacterial populations to adapt to unintended side effects without acquiring resistance to the anti-virulence effect itself.

To better understand these adaptations on a molecular level, the RC41-evolved populations were whole-genome sequenced, which revealed that all three RC41-treated biofilms acquired mutations related to RamR, a repressor of the AcrAB efflux system (Table 1; Fig. 2). Highly similar mutations in *ramR* are frequently identified in drug resistant isolates, resulting in AcrAB overexpression and thus elevated efflux levels[26,29–31]. For example, a similar mutation at the +2 position in the RamR binding site of the *ramA* promoter has been observed in a multidrug resistant (MDR) *S.* Typhimurium strain, possibly resulting in weaker interactions between RamR and the *ramA* promoter. The exact Trp185* mutation observed in RC41-evolved lineage 2 has also been found in a *Klebsiella pneumonia* population experimentally evolved with increasing tigecycline concentrations[45]. Additionally, a premature stop codon at position 160, that is reminiscent to the Trp185* mutation, has been reported to be causal for the MDR phenotype of another *S.* Typhimurium strain[26], while deletion of the final 22 amino acids of RamR has been demonstrated to confer resistance to various antibiotics due to overexpression of *ramA*[29]. Finally, in silico modeling has predicted that similar substitutions, in particular Tyr59His, decrease the DNA binding affinity of RamR to the *ramA* promoter[46]. Based on these observations, it seems likely that the deletion of the final stretch of amino acids in the RamR sequence in the Trp185* mutant disrupts the dimerization interface, hence causing a partial loss-of-function. Consistent with the observed *ramR* mutations, the RC41-evolved populations showed increased efflux levels comparable to that of a *ramR* deletion construct (Δ*ramR*) (Fig. 4).

Moreover, we found a substantial fitness advantage for *ramR* loss-of-function (Δ*ramR*) only in *Salmonella* biofilms treated with RC41 (Fig. 6). This suggests that increased efflux provides a benefit to *Salmonella* cells during RC41 treatment, likely by reducing intracellular RC41 levels and hence diminishing the unintended growth delay. Since the evolved *Salmonella* biofilms overcame the growth delay but not the EPS inhibition, this also implies that the anti-biofilm effect of RC41 is not affected by increased efflux levels. Our current hypothesis is that RC41, similar to other 2-aminoimidazoles[47], interacts with an extracellular target in the cell envelope. In the case of RC41, this interaction triggers a signaling cascade that finally results in the repression of *csgD*. This hypothesis is supported by the observation that 2-AI-based EPS inhibitors seem to retain their anti-biofilm activity even when covalently coated on a surface[18,21].

While anti-biofilm activity of RC41 remained unaffected, the observed increase in efflux in the RC41-evolved biofilms translated to low levels of cross-resistance to clinically relevant antibiotics, such as azithromycin and ciprofloxacin (Fig. 4). However, the observed increases in MIC remain well below the clinical breakpoints for *Salmonella* for both azithromycin (15 μg mL^{-1}) and ciprofloxacin (0.06 μg mL^{-1})[48]. This is consistent with previous reports demonstrating that efflux upregulation is only able to confer low levels of antibiotic resistance (2- to 8-fold MIC increases)[49]. Interestingly, efflux-related mutations are often a first step in the process of antibiotic resistance evolution. Since the upregulation of efflux is energetically costly and confers limited resistance, additional mutations often arise that more directly abolish the antimicrobial effect, allowing the costly efflux mutations to be reverted[49]. Efflux mutations selected during RC41 treatment could thus act as a stepping stone, facilitating the development of high levels of antibiotic resistance[49]. However, RC41 may simultaneously reduce the risk of antibiotic resistance development by inhibiting biofilms, which are inherently more tolerant to antibiotics[12] and could themselves act as a stepping stone towards antibiotic resistance[49]. In the case of resistance towards the growth-inhibitory effect of RC41, the increased efflux mutations were not replaced by more specific resistance mutations, even after 40 days of treatment. This is possibly because the upregulation of the AcrAB efflux system was not associated with a significant cost in our experimental setup (Supplementary Figs. 6–7).

To mitigate the potential risk of facilitating cross-resistance to antibiotics, we explored strategies to eliminate the unintended growth effects of RC41. One of the advantages of using 2-AI-based compounds as EPS inhibitors is that their properties can be fine-tuned through modification of the specific chemical groups on the 2-AI scaffold[20,23]. Chemical modification of the RC41 molecule improved the anti-biofilm activity while reducing the unintended growth defect and eliminating the fitness advantage of a *ramR* loss-of-function (Fig. 7). Despite these improvements, the chemical modification was not able to fully eliminate the growth delay. As a result, cells with increased efflux may still retain a slight fitness advantage that, while undetectable in our experimental setup, could enable the gradual enrichment of these mutations over time. Consequently, we cannot entirely rule out the possibility that long-term treatment with the modified EPS inhibitor might select for increased efflux and cross-resistance to antibiotics but with a strongly reduced selection pressure compared to RC41. Ongoing efforts aim to further screen chemically modified 2-AI-based EPS inhibitors to identify molecules for which the EPS inhibition and growth delay are fully uncoupled, thereby eliminating the selective pressure for increased efflux. In addition, applications in which the EPS inhibitors are covalently coated on a surface are being explored. Such coatings are expected to negate the risk of efflux-based cross-resistance, as the inhibitors remain surface-bound and cannot enter bacterial cells. Previous work has demonstrated that coating 2-AI-based EPS inhibitors on orthopedic implants retains their anti-biofilm activity[18,21]. Moreover, when the chemically modified EPS inhibitor (RC6) used here is covalently linked to iron oxide nanoparticles, the anti-biofilm effect is preserved while the unintended planktonic growth delay is fully eliminated (Sutens et al., in preparation). Thus, both chemical modification and covalent coating seem promising avenues to fully unlock the potential of 2-AI-based EPS inhibitors and minimize the risk of cross-resistance to antibiotics through efflux.

In conclusion, the development of anti-virulence drugs without unintended side effects that contribute to the development of resistance remains challenging. Nonetheless, our findings underscore the feasibility of this approach. While our EPS inhibitor inadvertently caused a growth delay that selected for increased efflux, this adaptation did not confer resistance to the anti-biofilm effect. Importantly, chemical modification of the EPS inhibitor successfully mitigated the unintended side effects while preserving its anti-virulence activity, highlighting the flexibility of 2-AI-based compounds as a platform for the development of EPS inhibitors. These results underscore both the advantages and the limitations of EPS inhibitors as an anti-virulence strategy. On one hand, the lack of resistance to the anti-biofilm effect supports their potential as evolutionarily robust therapeutics. On the other hand, the observed influence on bacterial adaptation, even in the absence of direct resistance to virulence inhibition, emphasizes the complexity of bacterial responses to such therapies.

Methods

Bacterial strains, plasmids, and growth conditions

All experiments were performed using the wild-type *Salmonella enterica* serovar Typhimurium ATCC14028 reference strain[50], and the isogenic Δ*ramR*, Δ*rpoS*, and Δ*ramR*Δ*rpoS* mutants. Both single mutants (Δ*ramR* and Δ*rpoS*) have been previously constructed and validated[51,52]. The Δ*ramR*Δ*rpoS* double mutant was constructed using P22 phage transduction[53], where the Δ*ramR* mutant acted as the acceptor strain and an *rpoS::KanR* mutant from the McClelland collection[54] was used as the donor strain. After successful transduction, the kanamycin resistance cassette was removed using the pCP20 plasmid encoding an FLP recombinase to obtain the Δ*ramR*Δ*rpoS* double mutant. Afterward, the pCP20 plasmid was cured using its temperature-sensitive origin of replication. Deletions were validated by PCR and Sanger sequencing.

To be able to differentiate between strains in competition experiments, the pFPv25.1_*gfpmut3* plasmid or the pFPv25.1_*dsRed.T4* plasmid were used[7]. These plasmids are identical, except for the fluorescent protein marker they encode, resulting in green (*gfpmut3*) and red (*dsRed.T4*) fluorescent colonies, respectively. These plasmids were electroporated into the desired *Salmonella* clones using a Bio-Rad Gene Pulser (Bio-Rad Laboratories). When these plasmids were used, 100 μg mL^{-1} ampicillin was added to the system to ensure plasmid maintenance.

Unless mentioned otherwise, stationary phase pre-cultures of the bacteria were prepared from single colonies in Lysogeny Broth (LB; 10 g L^{-1} NaCl, 10 g L^{-1} Tryptone, 5 g L^{-1} Yeast Extract) at 37 °C (200 rpm), while 20-fold diluted Tryptic Soy Broth (1:20 TSB; Fisher Scientific) was used for the experiments. If agar plates were needed, 15 g L^{-1} of bacteriological agar was added.

Chemicals

The 2-aminoimidazole-based EPS inhibitors (2-AI) that were used include 5-(4-chlorophenyl)-N-cyclopentyl-1H-imidazol-2-amine (RC41) (Supplementary Fig. 1A) and N-octylamine-5-(4-bromophenyl)-1H-imidazol-2-amine HCl (RC6) (Supplementary Fig. 1B). Their chemical synthesis has been described elsewhere[20,23]. These molecules were dissolved in dimethyl sulfoxide (DMSO) as a carrier solvent. Ciprofloxacin (Sigma), ampicillin (Sigma), and kanamycin (MP Biomedicals) were dissolved in dH_2O, while meropenem (TCI) and azithromycin (TCI) were dissolved in DMSO.

Quantification of planktonic and biofilm biomass

To quantify the effect of the EPS inhibitors on both planktonic and biofilm biomass, dose-response curves were determined using a Calgary Biofilm Device (CBD)[55]. First, a two-fold dilution series in 1:20 TSB of the EPS inhibitor or the carrier solvent (DMSO) was prepared inside the CBD system in a total volume of 100 μL per well. Next, pre-cultures of the desired bacterial strain or population were washed in Phosphate Buffered Saline (PBS; 1.24 g L^{-1} K_2HPO_4, 0.39 g L^{-1} KH_2PO_4, 8.8 g L^{-1} NaCl; pH 7.2) and normalized to an Optical Density at 595 nm (OD_{595nm}) of 3.2, which corresponds to approximately 10^9 cells mL^{-1}. After normalization, the cultures

were diluted 100-fold in 1:20 TSB, and 100 µL of this inoculum was mixed with the EPS inhibitor inside the CBD. The CBD system was then statically incubated at 25 °C for 48 h. After incubation, the planktonic biomass was quantified by measuring the OD_{595nm} inside the wells using a Synergy Mx plate reader (BioTek Instruments). Biofilm biomass on the pegs was quantified using crystal violet staining. Hereto pegs were first washed in 200 µL PBS and stained in 200 µL crystal violet (0.1%; dissolved in 1:1:18 isopropanol-methanol-PBS solution) for 30 min. Excess stain was removed in 200 µL dH_2O, after which the pegs were air-dried for 30 min. Afterward, the crystal violet stain was dissolved in 200 µL of a 30% acetic acid solution, and the OD_{570nm} was measured. To create dose-response graphs, the measured OD values were normalized relative to untreated controls. A similar assay was used to quantify planktonic biomass and biofilm biomass of the evolved populations (see below) in the presence and absence of an EPS inhibitor. Hereto, an identical procedure was followed, but pre-cultures were inoculated from the evolved population samples stored at −80 °C instead of using single colonies.

Serial passage evolution with an EPS inhibitor

To evaluate the evolutionary adaptations of *Salmonella* biofilms to long-term exposure to the 2-AI-based EPS inhibitor RC41, a serial passage evolution experiment was performed. Six parallel lineages, three treated with RC41 and three corresponding control lineages, were evolved for 20 two-day cycles. These lineages were inoculated using three independent bacterial pre-cultures that were normalized to an OD_{595nm} of 3.2 and diluted 100-fold in 10 mL 1:20 TSB. This inoculum was then divided into two parts of 5 mL, of which one was treated with 50 µM of RC41, while the other part served as a control. Both parts were then poured in separate small Petri dishes (Ø 60 mm) and were incubated statically at 25 °C for 48 h. After incubation, the liquid phase was gently discarded, and the biofilm cells adhering to the surface were recovered in 1 mL PBS using a cell scraper (Greiner). From the recovered biofilm cells, half the volume (500 µL) was diluted in 4.5 mL fresh 1:20 TSB, treated with 50 µM of RC41 if required, and inoculated in a new Petri dish. The remaining 500 µL biofilm cells were mixed with glycerol (25%) and stored at −80 °C. This process was repeated for 20 cycles.

Whole-genome sequencing of end-point populations

Whole-genome sequencing was performed on the end-point biofilm populations of the serial passage evolution experiment. Genomic DNA was recovered from these biofilm samples using the DNeasy Blood & Tissue Kit (Qiagen Benelux B.V.) according to the manufacturer's instructions. Purified DNA samples were sent to GENEWIZ Europe (Leipzig, Germany) for whole-genome sequencing. Initial data quality assessment was conducted using FastQC (v0.11.9) and aggregated using MultiQC (v1.12). Sequencing reads were aligned to the reference genome (NCBI reference sequence NC_016856.1) using Bowtie2 (2.4.1). Sorting and indexing of the output was performed using Samtools (v1.16). Variant calling was done using LoFreq (v2.1.3.1), and variant calls were annotated using SnpEff (v5.0).

Qualitative evaluation of catalase activity

To qualitatively evaluate catalase activity, pre-cultures of the desired *Salmonella* clones were washed in PBS and normalized to an OD_{595nm} of 2.5. The bacterial cell suspension was incubated for 15 min at 55 °C to inactivate the heat-labile *katG*-encoded catalase, which is not a part of the σ^S regulon. Next, 100 µL of the inoculum was transferred to a Pyrex test tube and mixed with 100 µL of a 1% Triton X-100 solution and 100 µL of a 30% hydrogen peroxide solution. Foam formation, which indicates catalase activity, was qualitatively assessed for each clone. Since *S.* Typhimurium only encodes two catalases (*katG* and *katE*), and KatG was heat-inactivated, foam formation indicates expression of *katE*, which is part of the σ^S regulon and thus requires a functional *rpoS* gene to be expressed[36].

PCR amplification and Sanger sequencing of *rpoS* and *rpoC*

To PCR amplify the *rpoS* and *rpoC* genes from the *Salmonella* genome, the high-fidelity Q5 polymerase (New England Biolabs) was used. The reaction mixtures (50 µL) and thermal cycling protocols were carried out according to the manufacturer's instructions. For amplification of *rpoS*, 5′-GCTGGCAGAAGACAAACGG was used as the forward primer and 5′-GTCAAGGGATCACGGGTAGG as the reverse primer. For amplification of *rpoC*, 5′-GTAAGCAGGGTCGTTTCC was used as the forward primer and 5′-CAGACCCAATACCACGTCC as the reverse primer. These primers were manufactured by Integrated DNA Technologies (IDT, Leuven, Belgium). After PCR amplification, the PCR products were mixed with BlueJuice (Thermo Fisher) and loaded on a 1% agarose gel supplemented with ethidium bromide. The gel was then submerged in Tris/Borate/EDTA (TBE) buffer, and gel electrophoresis was run for 1 h at 130 V and 500 mA, after which DNA fragments were visualized under UV light and compared to a SmartLadder (Eurogentec) as size reference. Fragments of interest were then excised from the gel and purified using the GelElute kit (Sigma) according to the manufacturer's instructions. Purified DNA fragments were sent for Sanger sequencing (Eurofins Genomics) using the Mix2Seq format in accordance with the provided guidelines. Obtained sequences were aligned with the corresponding wild-type reference sequence using Benchling.

Quantification of *csgD* expression through RT-qPCR

Population-level *csgD* expression was quantified using a real-time quantitative polymerase chain reaction (RT-qPCR). Population-level pre-cultures were directly inoculated from the evolved samples stored at −80 °C instead of from single colonies. After incubation, pre-cultures were normalized to an OD_{595nm} of 3.2 and diluted a hundred-fold in 1:20 TSB. Next, 5 mL of the inoculum was poured into a small Petri dish and incubated statically for 48 h at 25 °C. After incubation, the liquid phase was discarded, and the biofilm cells adhering to the surface were recovered using a cell scraper in 1.2 mL stop solution (200 µL of a 95% ethanol – 5% phenol mixture diluted in 1 mL TSB). Biofilm samples were snap-frozen in liquid nitrogen and stored at −80 °C until further use. RNA was extracted from these biofilm samples using the SV Total RNA Isolation System (Promega) and converted to cDNA using the RevertAid H Minus First Strand cDNA Synthesis Kit (Fisher Scientific) according to the manufacturer's instructions. cDNA levels were quantified with a StepOnePlus Real-Time PCR System (Applied Biosystems) using a SYBR Green probe (Bioline) and previously validated primers (Supplementary Table 1) for *csgD* and three housekeeping genes (*rpoD*, *rfaH*,*16 s rDNA*) for normalization. In brief, 5 µL of 1000-fold diluted cDNA samples were mixed with 10 µL SYBR Green, 3.2 µL nuclease-free water, and 0.9 µL of both forward and reverse primers (2 µM). These samples were submitted to a temperature cycling protocol consisting of an initial denaturation step (95 °C, 2′), followed by 40 cycles of denaturation (95 °C, 5″), annealing (60 °C, 30″), and elongation (72 °C, 15″). For each sample, *csgD* expression was normalized using the three selected housekeeping genes (Supplementary Table 1), and the fold change in normalized *csgD* expression was quantified relative to the wild-type samples using the ΔΔCt method[56].

Quantification of efflux through Nile Red staining

To evaluate the efflux activity of evolved *Salmonella* populations, an efflux assay with Nile Red was performed[57]. Population-level pre-cultures were directly inoculated from the evolved samples stored at −80 °C instead of from single colonies. After incubation, pre-cultures were concentrated to an OD_{595nm} of 10. Then, the cells were treated with 10 µM carbonyl cyanide m-chlorophenylhydrazone (CCCP) for 15 min. Afterward, 5 µM Nile Red was added. The cells were then incubated for 3 h at 37 °C (200 rpm) and 1 h at room temperature (static). After incubation, the samples were centrifuged for 5 min at 4400 rpm, the supernatant was discarded, and the pellet was resuspended in 20 mM Potassium Phosphate Buffer (PPB; 1.26 g L^{-1} KH_2PO_4, 1.87 g L^{-1} K_2HPO_4; pH 7) supplemented with 1 mM $MgCl_2$ and 50 µM RC41 or DMSO if required. The samples were diluted tenfold in a black 96-well glass-bottom plate with high-performance #1.5 cover glass, and the fluorescence (excitation 552 nm, emission 636 nm) was measured using a Synergy Mx plate reader for 2 min. To activate the efflux systems of

the bacteria, 50 mM glucose was added to the cells, and the fluorescence was monitored for another five minutes. For each sample, the fluorescence values were normalized relative to the fluorescence at $t = 0$ s. A one-phase exponential decay model was then used to fit the data, and the rate constant (K, s^{-1}) and half-life (s) were extracted[37].

$$\text{for } x < X_0 : y = Y_0 \quad (1)$$

$$\text{for } x \geq X_0 : y = P + (Y_0 - P)^* \exp(-K^*(x - X_0)) \quad (2)$$

In this model, x represents time (s), and y represents relative fluorescence. X_0 denotes the time (s) at which decay starts, i.e., when glucose is supplemented to the bacterial cultures. Y_0 is the average fluorescence up to X_0, so before decay starts. P is the asymptotic plateau value to which y converges if x becomes infinite. Finally, K denotes the rate constant (s^{-1}) of the exponential decay. The half-life (s) can then be computed as ln(2)/K and represents the time (s) required for the fluorescent signal to reach half of its initial value Y_0.

Determination of the Minimal Inhibitory Concentration

The Minimal Inhibitory Concentrations (MICs) of evolved *Salmonella* populations against azithromycin, ciprofloxacin, and meropenem were determined to quantify resistance levels against these antibiotics[58]. Population-level pre-cultures were directly inoculated from the evolved samples stored at −80 °C instead of from single colonies. After overnight incubation, pre-cultures were normalized to an OD_{595nm} of 0.1 in PBS and diluted 200-fold in 1:20 TSB, resulting in approximately 10^5 cells mL^{-1}. Then, a two-fold dilution series of the antibiotics was prepared in a 96-well plate, resulting in a final volume of 100 µL per well. These wells were then filled with 100 µL of the normalized bacterial suspension. A sterile control and growth control were included. Plates were then sealed with a BREATHseal membrane (Greiner) and incubated overnight at 37 °C (200 rpm), after which the OD_{595nm} was measured using a Synergy Mx plate reader. MIC values were determined by fitting a modified Gompertz model[59].

$$y = A + C^*e^{-e^{B(x-M)}} \quad (3)$$

In this model, x represents the log of the antimicrobial concentration, and y denotes the density of the bacterial cultures (OD_{595nm}). A is the lower asymptotic value of y, and C is the distance between the upper and lower asymptotes. Finally, B determines the slope, and M represents the x value at the inflection point. Based on this parameterization, the MIC can be computed as $10^{(M+1/B)}$, which gives the intersection of the lower asymptote of y and the tangent at the inflection point.

Analysis of growth curves

To evaluate the growth of the different strains and populations, growth was measured over time using the Bioscreen C system. First, the OD_{595nm} of pre-cultures was normalized to 2.5, after which normalized cultures were diluted 1000-fold in 1:20 TSB, resulting in approximately 10^6 cells mL^{-1}. If required, bacterial suspensions were supplemented with the appropriate concentration of the 2-AI-based EPS inhibitor (RC41 or RC6) or the carrier solvent (DMSO). Then, 200 µL of the inoculum was transferred to a Bioscreen plate, including at least three technical replicates for each sample. The plate was then placed inside the Bioscreen C system (Oy Growth Curves Ab Ltd.), and the OD_{600nm} was measured every 15 min for 24 h at 25 °C (shaken). To estimate exponential growth rates and lag times, a Zwietering-modified Gompertz model was fitted on the exponential growth phase (first 8–24 h depending on the treatment conditions)[40].

$$y = Y_m * e^{-e^{\frac{e*G}{Y_m}(L-x)+1}} \quad (4)$$

In this model, x represents time (h), and y represents the density of bacterial cultures (OD_{600nm}). Y_m denotes the upper asymptotic value of y. L represents the lag time, which can be interpreted as the timepoint at which bacterial growth commences and y reaches 6.6% of the maximal yield Y_m. Finally, G denotes the absolute growth rate, which can be interpreted as the tangent to the growth curve at the inflection point.

Biofilm competition experiments in small Petri dishes

To investigate the fitness effects of various mutations (Δ*ramR*, Δ*rpoS*, Δ*ramR*Δ*rpoS*) in biofilms treated with the EPS inhibitors, biofilm competition experiments in small Petri dishes were performed. First, the strains of interest were electroporated with pFPv25.1 containing either a green (*gfpmut3*) or red (*dsRed.T4*) fluorescent reporter. Next, pre-cultures of these fluorescently labeled strains were normalized to an OD_{595nm} of 3.2. Normalized cultures of both competitors were then diluted 100-fold in 5 mL 1:20 TSB in a 1:1 ratio. The inoculum was then supplemented with either DMSO or the EPS inhibitor and poured into a small Petri dish. Petri dishes were statically incubated for 48 h at 25 °C, after which the liquid phase was carefully removed, and biofilm cells were recovered in 1 mL PBS using a cell scraper. The obtained biofilm cells were then vortexed and passed through a syringe with a needle (25 G, 0.5 × 1.6 mm) five times to disrupt cell clusters and biofilm aggregates. Both the biofilm cells and the initial inoculum were diluted in PBS, and 100 µL was plated out on LB agar. Agar plates were incubated overnight at 37 °C, after which red and green colonies were counted using the Illumatool Tunable Lighting System (Lightools Research).

Statistical analysis

At least three independent biological repeats were acquired for each experiment. Statistical analyses were performed in GraphPad Prism (v10). To test for statistically significant differences, either a two-tailed Student's *t*-test, a one-way ANOVA, or a two-way ANOVA was used. Depending on the specific groups being compared, ANOVA analysis was followed up with a post-hoc multiple comparisons test using either Tukey's, Sidak's, or Dunnett's correction.

Reporting summary

Further information on research design is available in the Nature Research Reporting Summary linked to this article.

Data availability

The data that support the findings of this study are available from the corresponding author upon request. The raw sequencing reads obtained from the whole-genome sequencing of the evolved biofilm populations were deposited in the NCBI Sequence Read Archive (SRA) and can be accessed through the BioProject accession number PRJNA1224455.

Received: 2 October 2024; Accepted: 4 April 2025;
Published online: 06 May 2025

References

1. Darby, E. M. et al. Molecular mechanisms of antibiotic resistance revisited. *Nat. Rev. Microbiol.* **21**, 280–295 (2023).
2. Brepoels, P. et al. Antibiotic cycling affects resistance evolution independently of collateral sensitivity. *Mol. Biol. Evol.* **39**, msac257 (2022).
3. Jahn, L. J., Munck, C., Ellabaan, M. M. H. & Sommer, M. O. A. Adaptive laboratory evolution of antibiotic resistance using different selection regimes lead to similar phenotypes and genotypes. *Front. Microbiol.* **8**, 816 (2017).
4. Lindsey, H. A., Gallie, J., Taylor, S. & Kerr, B. Evolutionary rescue from extinction is contingent on a lower rate of environmental change. *Nature* **494**, 463–467 (2013).
5. Rasko, D. A. & Sperandio, V. Anti-virulence strategies to combat bacteria-mediated disease. *Nat. Rev. Drug Discov.* **9**, 117–128 (2010).
6. Dickey, S. W., Cheung, G. Y. C. & Otto, M. Different drugs for bad bugs: antivirulence strategies in the age of antibiotic resistance. *Nat. Rev. Drug Discov.* **16**, 457–471 (2017).

7. Dieltjens, L. et al. Inhibiting bacterial cooperation is an evolutionarily robust anti-biofilm strategy. *Nat. Commun.* **11**, 107 (2020).
8. Lissens, M., Joos, M., Lories, B. & Steenackers, H. P. Evolution-proof inhibitors of public good cooperation: a screening strategy inspired by social evolution theory. *FEMS Microbiol. Rev.* **46**, fuac019 (2022).
9. West, S. A., Griffin, A. S., Gardner, A. & Diggle, S. P. Social evolution theory for microorganisms. *Nat. Rev. Microbiol.* **4**, 597–607 (2006).
10. Costerton, J. W., Stewart, P. S. & Greenberg, E. P. Bacterial biofilms: a common cause of persistent infections. *Science* **284**, 1318–1322 (1999).
11. Kragh, K. N., Tolker-Nielsen, T. & Lichtenberg, M. The non-attached biofilm aggregate. *Commun. Biol.* **6**, 898 (2023).
12. Ciofu, O., Moser, C., Jensen, P, Ø. & Høiby, N. Tolerance and resistance of microbial biofilms. *Nat. Rev. Microbiol.* **20**, 621–635 (2022).
13. Miller, A. L. et al. In vivo synthesis of bacterial amyloid curli contributes to joint inflammation during S. Typhimurium infection. *PLoS Pathog* **16**, e1008591 (2020).
14. Tsuneda, S., Aikawa, H., Hayashi, H., Yuasa, A. & Hirata, A. Extracellular polymeric substances responsible for bacterial adhesion onto solid surface. *FEMS Microbiol. Lett.* **223**, 287–292 (2003).
15. El Hag, M. et al. Contribution of the csgA and bcsA genes to Salmonella enterica serovar Pullorum biofilm formation and virulence. *Avian Pathol. J. WVPA* **46**, 541–547 (2017).
16. Rainey, P. B. & Rainey, K. Evolution of cooperation and conflict in experimental bacterial populations. *Nature* **425**, 72–74 (2003).
17. Van Gestel, J., Weissing, F. J., Kuipers, O. P. & Kovács, Á. T. Density of founder cells affects spatial pattern formation and cooperation in Bacillus subtilis biofilms. *ISME J.* **8**, 2069–2079 (2014).
18. Coppola, G. A. et al. An improved 2-aminoimidazole based anti-biofilm coating for orthopedic implants: activity, stability, and in vivo biocompatibility. *Front. Microbiol*. **12**, 658521 (2021).
19. Jacobs, L. et al. 2-Aminoimidazoles as potent inhibitors of contaminating brewery biofilms. *Biofouling* **37**, 61–77 (2021).
20. Peeters, E. et al. Modulation of the substitution pattern of 5-aryl-2-aminoimidazoles allows fine-tuning of their antibiofilm activity spectrum and toxicity. *Antimicrob. Agents Chemother.* **60**, 6483–6497 (2016).
21. Peeters, E. et al. An antibiofilm coating of 5-aryl-2-aminoimidazole covalently attached to a titanium surface. *J. Biomed. Mater. Res. B Appl. Biomater.* **107**, 1908–1919 (2019).
22. Robijns, S. C. A. et al. A GFP promoter fusion library for the study of Salmonella biofilm formation and the mode of action of biofilm inhibitors. *Biofouling* **30**, 605–625 (2014).
23. Steenackers, H. P. L. et al. Structure-activity relationship of 2-hydroxy-2-aryl-2,3-dihydro-imidazo[1, 2-a]pyrimidinium salts and 2N-substituted 4(5)-aryl-2-amino-1H-imidazoles as inhibitors of biofilm formation by Salmonella Typhimurium and Pseudomonas aeruginosa. *Bioorg. Med. Chem.* **19**, 3462–3473 (2011).
24. Steenackers, H., Hermans, K., Vanderleyden, J. & De Keersmaecker, S. C. J. Salmonella biofilms: an overview on occurrence, structure, regulation and eradication. *Food Res. Int.* **45**, 502–531 (2012).
25. Ricci, V., Busby, S. J. W. & Piddock, L. J. V. Regulation of RamA by RamR in Salmonella enterica serovar Typhimurium: isolation of a RamR superrepressor. *Antimicrob. Agents Chemother.* **56**, 6037–6040 (2012).
26. Abouzeed, Y. M., Baucheron, S. & Cloeckaert, A. ramR mutations involved in efflux-mediated multidrug resistance in Salmonella enterica serovar Typhimurium. *Antimicrob. Agents Chemother.* **52**, 2428–2434 (2008).
27. Nikaido, E., Yamaguchi, A. & Nishino, K. AcrAB multidrug efflux pump regulation in Salmonella enterica serovar Typhimurium by RamA in response to environmental signals. *J. Biol. Chem.* **283**, 24245–24253 (2008).
28. Eaves, D. J., Ricci, V. & Piddock, L. J. V. Expression of acrB, acrF, acrD, marA, and soxS in Salmonella enterica serovar Typhimurium: role in multiple antibiotic resistance. *Antimicrob. Agents Chemother.* **48**, 1145–1150 (2004).
29. Hentschke, M., Christner, M., Sobottka, I., Aepfelbacher, M. & Rohde, H. Combined ramR mutation and presence of a Tn1721-associated tet(A) variant in a clinical isolate of Salmonella enterica serovar Hadar resistant to tigecycline. *Antimicrob. Agents Chemother.* **54**, 1319–1322 (2010).
30. Hentschke, M., Wolters, M., Sobottka, I., Rohde, H. & Aepfelbacher, M. ramR mutations in clinical isolates of Klebsiella pneumoniae with reduced susceptibility to tigecycline. *Antimicrob. Agents Chemother.* **54**, 2720–2723 (2010).
31. Kehrenberg, C., Cloeckaert, A., Klein, G. & Schwarz, S. Decreased fluoroquinolone susceptibility in mutants of Salmonella serovars other than Typhimurium: detection of novel mutations involved in modulated expression of ramA and soxS. *J. Antimicrob. Chemother.* **64**, 1175–1180 (2009).
32. Lee, S. J. & Gralla, J. D. Promoter use by ς38 (*rpoS*) RNA polymerase. *J. Biol. Chem.* **277**, 47420–47427 (2002).
33. Zuo, Y., Wang, Y. & Steitz, T. A. The mechanism of E. coli RNA polymerase regulation by ppGpp is suggested by the structure of their complex. *Mol. Cell* **50**, 430–436 (2013).
34. Dalebroux, Z. D. & Swanson, M. S. ppGpp: magic beyond RNA polymerase. *Nat. Rev. Microbiol.* **10**, 203–212 (2012).
35. Lories, B. et al. Biofilm bacteria use stress responses to detect and respond to competitors. *Curr. Biol.* **30**, 1231–1244.e4 (2020).
36. Iwase, T. et al. A simple assay for measuring catalase activity: a visual approach. *Sci. Rep.* **3**, 3081 (2013).
37. Iyer, R., Ferrari, A., Rijnbrand, R. & Erwin, A. L. A fluorescent microplate assay quantifies bacterial efflux and demonstrates two distinct compound binding sites in AcrB. *Antimicrob. Agents Chemother.* **59**, 2388–2397 (2015).
38. Dhillon, S. Meropenem/vaborbactam: a review in complicated urinary tract infections. *Drugs* **78**, 1259–1270 (2018).
39. Saw, H. T. H., Webber, M. A., Mushtaq, S., Woodford, N. & Piddock, L. J. V. Inactivation or inhibition of AcrAB-TolC increases resistance of carbapenemase-producing Enterobacteriaceae to carbapenems. *J. Antimicrob. Chemother.* **71**, 1510–1519 (2016).
40. Tjørve, K. M. C. & Tjørve, E. The use of Gompertz models in growth analyses, and new Gompertz-model approach: an addition to the Unified-Richards family. *PLoS ONE* **12**, e0178691 (2017).
41. Roy, R., Tiwari, M., Donelli, G. & Tiwari, V. Strategies for combating bacterial biofilms: a focus on anti-biofilm agents and their mechanisms of action. *Virulence* **9**, 522–554 (2018).
42. Rezzoagli, C., Wilson, D., Weigert, M., Wyder, S. & Kümmerli, R. Probing the evolutionary robustness of two repurposed drugs targeting iron uptake in Pseudomonas aeruginosa. *Evol. Med. Public Health* **2018**, 246–259 (2018).
43. Maeda, T. et al. Quorum quenching quandary: resistance to antivirulence compounds. *ISME J.* **6**, 493–501 (2012).
44. Jeon, A. B. et al. 2-aminoimidazoles collapse mycobacterial proton motive force and block the electron transport chain. *Sci. Rep.* **9**, 1513 (2019).
45. Fang, L. et al. Step-wise increase in tigecycline resistance in Klebsiella pneumoniae associated with mutations in ramR, lon and rpsJ. *PLoS ONE* **11**, e0165019 (2016).
46. Liu, Y.-Y. & Chen, C.-C. Computational analysis of the molecular mechanism of RamR mutations contributing to antimicrobial resistance in Salmonella enterica. *Sci. Rep.* **7**, 13418 (2017).
47. Zeczycki, T. N. et al. 2-Aminoimidazole analogs target PhoP altering DNA binding activity and affect outer membrane stability in gram-negative bacteria. *Biochemistry* **61**, 2948–2960 (2022).
48. EUCAST. EUCAST: Clinical breakpoints and dosing of antibiotics. https://www.eucast.org/clinical_breakpoints (2024).

49. Singh, R. et al. Temporal interplay between efflux pumps and target mutations in development of antibiotic resistance in Escherichia coli. *Antimicrob. Agents Chemother.* **56**, 1680–1685 (2012).
50. Jarvik, T., Smillie, C., Groisman, E. A. & Ochman, H. Short-term signatures of evolutionary change in the Salmonella enterica serovar Typhimurium 14028 genome. *J. Bacteriol.* **192**, 560–567 (2010).
51. Akanksha, D. Evolutionary dynamics of resistance development against a biofilm inhibitor in Salmonella Typhimurium. [Doctoral dissertation, KU Leuven]. https://lirias.kuleuven.be/1759553&lang=en (2014).
52. Kim, H. Functional genome-wide analysis of Salmonella Typhimurium biofilm formation. [Doctoral dissertation, KU Leuven]. https://lirias.kuleuven.be/1759370&lang=en (2011).
53. Malke, H. R. W., Davis, D., Botstein & Roth, J. R. A manual for genetic engineering, advanced bacterial genetics. 251 S., 15 Abb. Cold Spring Harbor 1980. Cold Spring Harbor Laboratory. $ 28.20. *Z. Für Allg. Mikrobiol.* **21**, 767–767 (1981).
54. Porwollik, S. et al. Defined single-gene and multi-gene deletion mutant collections in Salmonella enterica sv Typhimurium. *PLoS ONE* **9**, e99820 (2014).
55. Ceri, H. et al. The Calgary Biofilm Device: new technology for rapid determination of antibiotic susceptibilities of bacterial biofilms. *J. Clin. Microbiol.* **37**, 1771–1776 (1999).
56. Hellemans, J., Mortier, G., De Paepe, A., Speleman, F. & Vandesompele, J. qBase relative quantification framework and software for management and automated analysis of real-time quantitative PCR data. *Genome Biol.* **8**, R19 (2007).
57. Bohnert, J. A., Karamian, B. & Nikaido, H. Optimized Nile Red Efflux Assay of AcrAB-TolC multidrug efflux system shows competition between substrates. *Antimicrob. Agents Chemother.* **54**, 3770–3775 (2010).
58. Wiegand, I., Hilpert, K. & Hancock, R. E. W. Agar and broth dilution methods to determine the minimal inhibitory concentration (MIC) of antimicrobial substances. https://doi.org/10.1038/nprot.2007.521 (2008).
59. Lambert, R. J. W. & Pearson, J. Susceptibility testing: accurate and reproducible minimum inhibitory concentration (MIC) and non-inhibitory concentration (NIC) values. *J. Appl. Microbiol.* **88**, 784–790 (2000).
60. Yamasaki, S. et al. The crystal structure of multidrug-resistance regulator RamR with multiple drugs. *Nat. Commun.* **4**, 2078 (2013).
61. Zuo, Y., De, S., Feng, Y. & Steitz, T. A. Structural insights into transcription initiation from de novo RNA synthesis to transitioning into elongation. *iScience* **23**, 101445 (2020).

Acknowledgements

This work was supported by the KU Leuven Research Council (C14/22/077, C3/20/081, PDMT2/22/039), the Fonds Wetenschappelijk Onderzoek-Vlaanderen (FWO) (3G045620, 3G046318, 1S85623N, G046318N, W000921N), the UGent BOF (BOF 01J06219, BOF/IOP/2022/045BOF), the Agentschap innoveren & Ondernemen (VLAIO) (HBC.2020.2902), the RUDN strategic academic leadership program (recipient E.V.d.E), and the H2020-MSCA-ITN-2016-BIOCLEAN project (grant agreement no. 722871). The funder played no role in the study design, data collection, analysis and data interpretation, or the writing of the manuscript.

Author contributions

M.J. and S.V.G. established the hypothesis, conducted the microbiological work, analyzed the data, and prepared the original draft. X.V. performed the serial passage evolution experiment. M.D. assisted in the microbiological work. G.C. synthesized the EPS inhibitor. C.A.P.R. and K.M. performed the whole-genome sequencing. B.L. and H.S. contributed to the manuscript revisions. T.V., B.L., and H.S. contributed to establishing the hypothesis. E.V.d.E., K.M., and H.S. provided financial support and supervision. M.J. and S.V.G. both contributed equally to this manuscript and are co-first authors. B.L. and H.S. share last authorship. All authors reviewed and approved the final manuscript.

Competing interests

The authors declare no competing interests.

Additional information

Supplementary information The online version contains supplementary material available at https://doi.org/10.1038/s41522-025-00693-y.

Correspondence and requests for materials should be addressed to Hans P. Steenackers.